ANTIOXIDANTS & REDOX SIGNALING
Volume 30, Number 15, 2019

DOI: 10.1089/ars.2018.7514

Discoveries

ORIGINAL RESEARCH COMMUNICATION

Endothelial Stanniocalcin 1 Maintains Mitochondrial Bioenergetics and Prevents Oxidant-Induced Lung Injury *via* Toll-Like Receptor 4

Yi Zhang,[1] Peiying Shan,[1] Anup Srivastava,[1,2] Zhenyu Li,[1,3] and Patty J. Lee[1]

Abstract

Aims: Oxidant-induced endothelial injury plays a critical role in the pathogenesis of acute lung injury (ALI) and subsequent respiratory failure. Our previous studies revealed an endogenous antioxidant and protective pathway in lung endothelium mediated by heat shock protein 70 (Hsp70)–toll-like receptor 4 (TLR4) signaling. However, the downstream effector mechanisms remained unclear. Stanniocalcin 1 (STC1) has been reported to mediate antioxidant responses in tissues such as the lungs. However, regulators of STC1 expression as well as its physiological function in the lungs were unknown. We sought to elucidate the relationship between TLR4 and STC1 in hyperoxia-induced lung injury *in vitro* and *in vivo* and to define the functional role of STC1 expression in lung endothelium.
Results: We identified significantly decreased STC1 expression in TLR4 knockout mouse lungs and primary lung endothelium isolated from TLR4 knockout mice. Overexpression of STC1 was associated with endothelial cytoprotection, whereas decreased or insufficient expression was associated with increased oxidant-induced injury and death. An Hsp70-TLR4-nuclear factor kappa-light-chain-enhancer of activated B cells (NFκB) signal mediates STC1 induction in the lungs and endothelial cells. We also demonstrated a previously unrecognized role for mitochondrial-associated STC1, *via* TLR4, in maintaining normal glycolysis, mitochondrial bioenergetics, and mitochondrial calcium levels.
Innovation: To date, a physiological role for STC1 in oxidant-induced ALI has not been identified. In addition, our studies show that STC1 is regulated by TLR4 and exerts lung and endothelial protection in response to sterile oxidant-induced lung injury.
Conclusions: Our studies reveal a novel TLR4-STC1-mediated mitochondrial pathway that has homeostatic as well as oxidant-induced cytoprotective functions in lung endothelium. *Antioxid. Redox Signal.* 30, 1775–1796.

Keywords: lung, mitochondria, endothelium, stanniocalcin

Introduction

ANIMAL MODELS HAVE DEMONSTRATED that excessive levels of inhaled oxygen, hyperoxia, lead to elevated levels of oxidants that damage both pulmonary epithelial and endothelial cells, thereby causing increased pulmonary capillary permeability, inflammation, and eventual respiratory demise—consistent with clinical acute lung injury (ALI). Our previous study showed that the innate immune receptor, toll-like receptor 4 (TLR4), confers protection against hyperoxia-induced

Innovation

Oxidant-induced endothelial injury plays a critical role in the pathogenesis of acute lung injury (ALI) and subsequent respiratory failure, yet specific therapies do not exist. We identified a mitochondrial-enriched antioxidant protein and its immune regulator in the lungs and endothelium that protects against ALI and death. Our studies identify new approaches and new therapies against ALI.

[1]Section of Pulmonary, Critical Care and Sleep Medicine, Yale University School of Medicine, New Haven, Connecticut.
[2]Division of Endocrinology, Department of Medicine, College of Medicine, University of Arizona, Tucson, Arizona.
[3]Intensive Care Unit, The Second Hospital of Tianjin Medical University, Tianjin, China.

lung and endothelial injury. We also found that the antioxidant and antiapoptotic functions of TLR4 in lung endothelium depend on an endogenous, soluble, TLR4 ligand heat shock protein 70 (Hsp70). However, the effector mechanisms and impact on endothelial function remained poorly understood. We sought to identify the mediators downstream of TLR4 signaling and the cellular mechanisms whereby TLR4 signaling exerts antioxidant and endothelial-protective effects in hyperoxia-induced acute lung injury (HALI).

Stanniocalcin 1 (STC1) is a glycoprotein, which was originally identified as a calcium-regulating hormone in fish (35). In mammals, the STC1 gene is widely expressed in tissues such as the lungs. *STC1* has both autocrine and paracrine effects to maintain calcium homeostasis and to inhibit apoptosis. Its localization in the spleen and thymus suggests a role in the immune/inflammatory responses (30).

Mitochondrial-associated STC1 has been reported to mediate antioxidant responses in macrophages and endothelial cells (30). STC1 is also thought to suppress reactive oxygen species (ROS) generation *via* uncoupling protein 2 (UCP2) induction (36). STC1 has angiogenic effects on endothelium in response to growth factors (46). STC1 promotes wound healing in epithelial cells (5), inhibits the activation of the innate immune system (27), and may promote the early inhibition of vascular leakage and re-epithelialization in damaged alveolar spaces (16).

Our present studies show that STC1 is associated with the innate immune receptor, TLR4, and promotes lung endothelial protection *in vitro* and *in vivo*. STC1 was significantly decreased in *TLR4*$^{-/-}$ mice and murine lung endothelial cells (MLECs). STC1 silencing phenocopied the mitochondrial and glycolysis dysfunction observed in *TLR4*$^{-/-}$ MLECs. The overexpression of STC1 with lentivirus vector in *TLR4*$^{-/-}$ restored the glycolytic and mitochondrial profiles to that of wild-type (WT) MLECs. Therefore, we identified a novel TLR4-STC1-mediated mitochondrial-protective pathway.

Results

Decreased antioxidant STC1 in TLR4$^{-/-}$ *mice and MLECs*

Our previous study showed that TLR4 confers protection against HALI and endothelial cell injury. During our investigations of lung-protective molecules after hyperoxia, we identified that specific heat shock proteins signaled *via* TLR4 (45). To identify candidate mechanisms downstream of TLR4, we performed microarray analyses on primary MLECs isolated from *TLR4*$^{-/-}$ and WT mice and identified a significant decrease in gene expression of *STC1* in *TLR4*$^{-/-}$ MLECs (Fig. 1A). In fact, *STC1* was one of the 26 genes that was different by at least 1.5-fold in knockout *versus* WT MLECs, $p < 0.05$ in microarray analyses (Supplementary Fig. S1). We confirmed decreased *STC1* mRNA in *TLR4*$^{-/-}$ MLECs compared with WT MLECs (Fig. 1B) and decreased STC1 protein levels in total lungs isolated from *TLR4*$^{-/-}$ mice compared with WT mice (Fig. 1C).

We sought to determine the relevant cell type involved in mediating STC1 effects. Our previous MLEC data pointed to an important role for endothelial cells during HALI. We evaluated lung sections of WT mice using STC1 and endothelial-specific antibody, cluster of differentiation 31 (CD31). STC1-immunoreactive cells (red conjugate) were

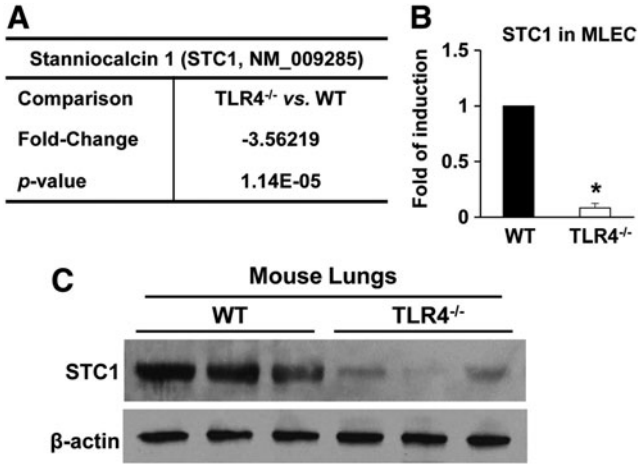

FIG. 1. STC1 is decreased in *TLR4*$^{-/-}$ MLECs and mice. (A) Affymetrix microarray analysis for *STC1* in primary isolated MLECs (experiments were performed in triplicate). Data are expressed as mean in the fold of change and *p*-value and analyzed by unpaired Student's *t* test, multiple testing correction with the method of Benjamini–Hochberg, *TLR4*$^{-/-}$ *vs* WT MLECs. **(B)** *STC1* mRNA expression in WT or *TLR4*$^{-/-}$ MLECs was measured by real-time RT-PCR and analyzed by the Mann–Whitney test. $*p < 0.05$ *vs* WT (experiments were performed in triplicate). **(C)** Total lung lysates isolated from 3-month-old WT or *TLR4*$^{-/-}$ mice were immunoblotted against STC1 antibody. β-Actin was used as protein loading control. See Supplementary Figure S9A for uncut gel. MLECs, mouse lung endothelial cells; RT-PCR, reverse transcription-polymerase chain reaction; STC1, stanniocalcin 1; TLR4, toll-like receptor 4; WT, wild type.

detected specifically in the blood vessels. Cells that were immunostained with surfactant protein C (SP-C), CC10, or alpha smooth muscle actin (αSMA) antibodies did not exhibit significant expression of STC1 (Fig. 2A and Supplementary Fig. S2A). These data indicated that STC1 appeared to be predominantly expressed in endothelium in WT lungs. We also found that the lungs from *TLR4*$^{-/-}$ mice were virtually absent of STC1 protein (Fig. 2B and Supplementary Fig. S2B).

Hyperoxia regulates STC1 in MLECs

STC1 has been reported to be involved in oxidative stress responses (30, 36) and in governing cellular survival and proliferation (46). Little is known about the regulation of STC1, and its function in the lungs has not been previously described. We were interested in determining the lung consequences of TLR4 deficiency during sterile oxidant stress, which led to our previous report of *TLR4*$^{-/-}$ mice having increased susceptibility to HALI and death (41). We found that STC1 protein and mRNA expression were induced in WT and *TLR4*$^{-/-}$ MLECs after hyperoxia. We confirmed that WT MLECs had more STC1 protein and mRNA expression at baseline and after hyperoxia compared with *TLR4*$^{-/-}$ MLECs (Fig. 3A, B). Therefore, hyperoxia-induced STC1 expression was dependent on TLR4 signaling.

STC1 is protective during hyperoxia in MLECs

To determine the physiological role of STC1, specifically in *TLR4*$^{-/-}$ MLECs, we performed loss-of-function (lenti-

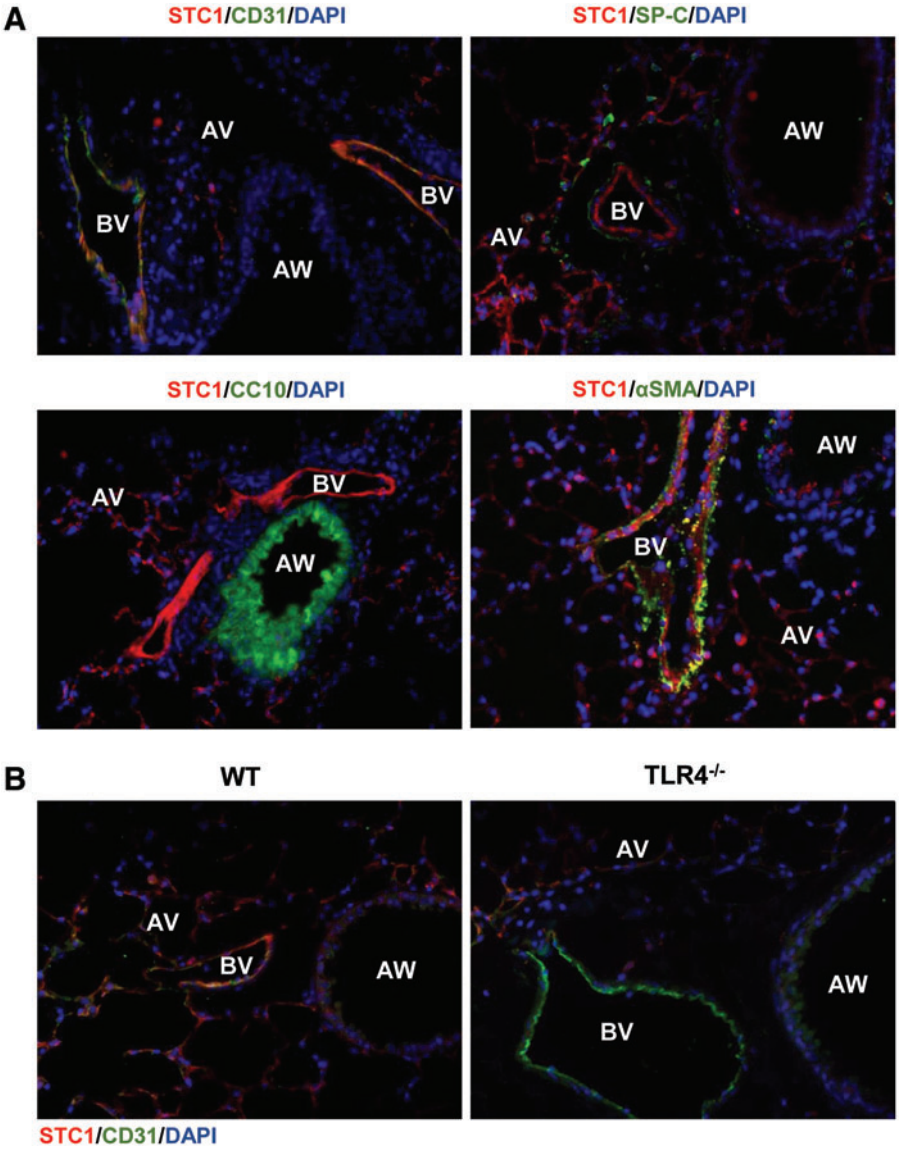

FIG. 2. STC1 localizes to lung endothelium *in vivo*. **(A)** Immunostains for STC1 (*red*) and CD31 (blood vessel endothelium marker, *green*), SP-C (alveolar type-II cell marker, *green*), CC10 (airway marker, *green*), or αSMA (*green*) with DAPI-stained nuclei (*blue*). The images are shown with all colors (All Channels) merged. The separate channel images were shown in Supplementary Figure S2. **(B)** Immunostains of lung tissue from WT or *TLR4*$^{-/-}$ mice for STC1 (*red*), CD31 (*green*), and DAPI-stained nuclei. The separate channel images are shown in Supplementary Figure S2. Original magnification of all photomicrographs: ×400. αSMA, alpha smooth muscle actin; AV, alveolar; AW, airway; BV, blood vessel; CD31, cluster of differentiation 31; DAPI, 4′,6-diamidino-2-phenylindole; SP-C, surfactant protein C. Color images are available online.

FIG. 3. STC1 is protective in MLECs during hyperoxia, which is dependent on TLR4. WT and *TLR4*$^{-/-}$ MLECs were exposed to 72 h of hyperoxia or RA as control. **(A)** Lysates were isolated and immunoblotted against STC1 antibody. β-Actin was used as protein loading control. Uncut gels are shown in Supplementary Figure S9B. **(B)** *STC1* mRNA expression was measured by real-time RT-PCR. *$p < 0.05$ *vs* WT RA; **$p < 0.05$ *vs* corresponding WT; $^{\#}p < 0.05$ *vs* *TLR4*$^{-/-}$ RA (experiments were performed in triplicates). WT or *TLR4*$^{-/-}$ MLECs were treated with lentivirus (lenti-Ctrl, lenti-STC1sh, knockdown of STC1, or STC1 overexpression lenti-STC1oe) and exposed to 72 h of hyperoxia or RA as control. Manipulation of STC1 expression by lentivirus was shown in Supplementary Figure S3. Graphical quantitation of flow cytometry analysis of apoptosis, the mean ± SD was determined in **(C)**. The representative *dot plots* out of the three experiments are shown in Supplementary Figure S4. The LDH activity was determined in **(D)**. H_2O_2 generation was determined by CM-H2DCFDA **(E)**, and mitochondrial ROS was determined by MitoSOX Red **(F)** levels. **(G)** WT or *TLR4*$^{-/-}$ MLECs were pretreated with hSTC1 (100 ng/mL) for overnight and exposed to 72 h of hyperoxia or RA as control. DHE staining was analyzed with fluorescence microscopy and quantified using the ImageJ software. Images are representative of five independent experiments. Scale bars = 100 μm. The relative DHE values are expressed as mean ± SD. *$p < 0.05$ *vs* WT lenti-Ctrl RA; **$p < 0.05$ *vs* corresponding Ctrl; $^{\#}p < 0.05$ *vs* corresponding RA; $^{\#\#}p < 0.05$ *vs* corresponding hyperoxia (experiments were performed in triplicates). Data were analyzed by two-way ANOVA with *post hoc* Tukey's HSD test calculator for multiple comparisons. ANOVA, analysis of variance; DHE, dihydroethidium; HSD, honestly significant difference; LDH, lactate dehydrogenase; RA, room air; ROS, reactive oxygen species; SD, standard deviation; sh, silencing RNA. Color images are available online.

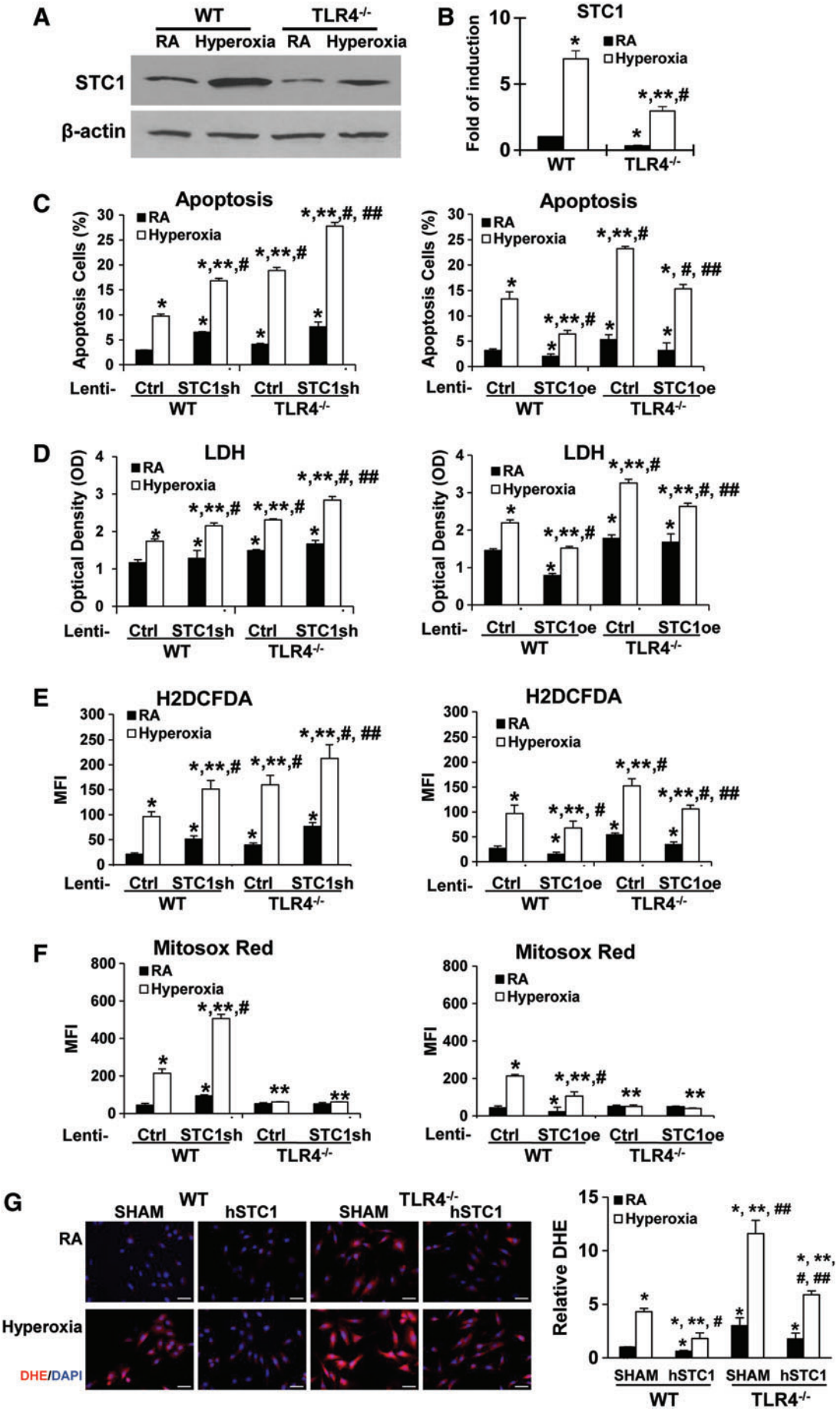
A
WT
TLR4-/-
RA
Hyperoxia
RA
Hyperoxia
STC1
β-actin
B
STC1
Fold of induction
RA
Hyperoxia
WT
TLR4-/-
C
Apoptosis
Apoptosis Cells (%)
RA
Hyperoxia
Lenti-
Ctrl
STC1sh
Ctrl
STC1sh
WT
TLR4-/-
Apoptosis
Apoptosis Cells (%)
RA
Hyperoxia
Lenti-
Ctrl
STC1oe
Ctrl
STC1oe
WT
TLR4-/-
D
LDH
Optical Density (OD)
RA
Hyperoxia
Lenti-
Ctrl
STC1sh
Ctrl
STC1sh
WT
TLR4-/-
LDH
Optical Density (OD)
RA
Hyperoxia
Lenti-
Ctrl
STC1oe
Ctrl
STC1oe
WT
TLR4-/-
E
H2DCFDA
MFI
RA
Hyperoxia
Lenti-
Ctrl
STC1sh
Ctrl
STC1sh
WT
TLR4-/-
H2DCFDA
MFI
RA
Hyperoxia
Lenti-
Ctrl
STC1oe
Ctrl
STC1oe
WT
TLR4-/-
F
Mitosox Red
MFI
RA
Hyperoxia
Lenti-
Ctrl
STC1sh
Ctrl
STC1sh
WT
TLR4-/-
Mitosox Red
MFI
RA
Hyperoxia
Lenti-
Ctrl
STC1oe
Ctrl
STC1oe
WT
TLR4-/-
G
WT
TLR4-/-
SHAM
hSTC1
SHAM
hSTC1
RA
Hyperoxia
DHE/DAPI
Relative DHE
RA
Hyperoxia
SHAM
hSTC1
SHAM
hSTC1
WT
TLR4-/-

STC1sh [silencing RNA]) and gain-of-function (lenti-STC1oe, overexpression vector) studies using lentivirus (Fig. 3C–F). We confirmed the efficiency of these STC1 expression manipulations by protein detection, as shown in Supplementary Figure S3A and B. Knockdown of STC1 by lenti-STC1sh in WT and *TLR4*$^{-/-}$ MLECs showed increased hyperoxia-induced apoptosis and lactate dehydrogenase (LDH) release (Fig. 3C, D, left panel; Supplementary Fig. S4). Lenti-STC1sh also increased oxidant generation induced by hyperoxia exposure compared with lenti-Ctrl silencing RNA (sh) (Fig. 3E, left panel). The overexpression of STC1 with lenti-STC1oe decreased hyperoxia-induced cell apoptosis, cellular LDH release, and oxidant production (Fig. 3C–E, right panel; Supplementary Fig. S4).

Given that mitochondria are a major source of ROS generation, we measured the mitochondrial ROS in MLECs using MitoSOX Red, a fluorescent dye that detects mitochondrial superoxide. Lenti-STC1 short hairpin RNA (shRNA) treatment led to increased hyperoxia-induced mitochondrial superoxide generation in WT MLECs (Fig. 3F, left panel). Lenti-STC1oe significantly inhibited hyperoxia-induced mitochondrial superoxide in WT MLECs (Fig. 3F, right panel). Interestingly, we found that MitoSOX Red levels were significantly lower in *TLR4*$^{-/-}$ MLECs at baseline and after hyperoxia (Fig. 3F). Moreover, the MitoSOX Red levels had not been influenced by *STC1* gene manipulation in *TLR4*$^{-/-}$ MLECs.

These findings suggested that STC1 might play a critical role in mitochondrial superoxide generation, which could influence the cell fate during hyperoxia. *TLR4*$^{-/-}$ MLECs might have dysfunctional mitochondria; therefore, it had less mitochondrial superoxide generation and maintained the mitochondrial superoxide at lower levels compared with WT MLECs. We also performed dihydroethidium (DHE) staining as a general measure of cytosolic superoxide levels in live cells. As shown in Figure 3G, recombinant human STC1 protein decreased hyperoxia-induced oxidant production as measured by the DHE staining in both WT and *TLR4*$^{-/-}$ MLECs. Interestingly, we detected exogenously delivered hSTC1 in mitochondria. Endocytosis inhibitor, Pitstop 2, appeared to block the exogenous hSTC1 uptake (Supplementary Fig. S5).

Hsp70-TLR4-NFκB signal mediates STC1 induction

We reported that soluble Hsp70 can function as an endogenous TLR4 ligand, *via* the TLR4 adaptor protein, Trif (TIR-domain-containing adapter-inducing interferon-β), and NFκB (nuclear factor kappa-light-chain-enhancer of activated B cells) during HALI (45). To investigate whether the Hsp70-TLR4-NFκB signal regulated the *STC1* expression, we treated WT MLECs with lenti-STC1sh or its lenti-Ctrl, combined with Hsp70 overexpression adenoviral Hsp70 (Ad-Hsp70) or adenovirus-control (CMV-null) (Ad-Ctrl), before 72 h of hyperoxia. We confirmed that both Hsp70 overexpression and hyperoxia induced STC1 protein and mRNA expression (Fig. 4A, B). As we reported previously (45), Ad-Hsp70 decreased hyperoxia-induced cell injury in WT MLECs, as assessed by an apoptosis assay (Fig. 4C, Supplementary Fig. S6A), as well as LDH release (Fig. 4D). Knockdown of STC1 with STC1shRNA increased hyperoxia-induced cell apoptosis and LDH release (Fig. 4C, D), and the inhibition of apoptosis by Ad-Hsp70 during hyperoxia was dependent on the level of STC1.

Next, we sought to determine the ability of TLR4 to specifically regulate STC1 in MLECs. We recently reported the efficiency and specificity of our TLR4 lentiviral constructs (33, 44). We performed loss-of-function experiments by using all-cell and Ec-targeting TLR4 silencing constructs (TLR4shRNA or VE-TLR4shRNA, respectively). We found that TLR4 silencing significantly decreased STC1 expression compared with lenti-Ctrl before and after hyperoxia (Fig. 4E). We also found that Ad-Hsp70 could not induce STC1 protein or mRNA expression in *TLR4*$^{-/-}$ MLECs (Fig. 4F, G). Taken together, these data show that STC1 induction is regulated by TLR4 in lung endothelium and prevents lethal pro-oxidant lung injury.

In addition, we investigated a specific role for endothelial NFκB in regulating STC1. The promoter of human STC1 contains multiple NFκB p65 binding sites, as reported previously (13). We found that the knockdown of the p65 subunit in NFκB by p65 small interfering RNA (siRNA) abolished Ad-Hsp70-induced STC1 protein and mRNA expression (Fig. 5A, B).

We performed the electromobility shift assay (EMSA) by using NFκB binding sites to confirm extracellular Hsp70-mediated TLR4 signaling. Ad-Hsp70 or hyperoxia alone led to NFκB activation in WT and *Hsp70*$^{-/-}$ MLECs, which was abolished in *TLR4*$^{-/-}$ MLECs (Fig. 5C). We also found that the NFκB inhibitor, CAY 10512, abolished Ad-Hsp70 and hyperoxia-mediated STC1 protein and mRNA induction (Fig. 5D, E). Meanwhile, CAY 10512 also abolished the protective effects of Ad-Hsp70 during hyperoxia, as assessed by apoptosis analysis and cellular LDH release measurements (Fig. 5F, G; Supplementary Fig. S6B). Therefore, Hsp70 acts as a TLR4-dependent ligand and utilizes a NFκB-STC1 signal to promote endothelial cell survival in basal and hyperoxic conditions.

STC1 is expressed predominantly in mitochondria of MLECs at baseline and after hyperoxia

To more precisely understand the mechanism of STC1-mediated antioxidant and protective effects in endothelium, we investigated the cellular location of STC1. Filvaroff *et al.* found enlarged myocyte mitochondria, with normal structure and organized cristae, in STC1 transgenic mice compared with the age-matched WT mice (11). Huang *et al.* also found mitochondrial changes after STC1 knockdown (17). These reports suggested a potential association between STC1 and mitochondria. First, we performed colocalization immunostaining for STC1 and specific intracellular organelles (Hsp60 for mitochondria, Golgin-97 for Golgi, and ERp72 for endoplasmic reticulum [ER]) and observed the greatest number of merged (yellow) areas for Hsp60, consistent with mitochondrial localization (Fig. 6A). We quantified a colocalization coefficient by calculating the fraction of overlapping signals (8), as shown in the right panel of Figure 6A.

To confirm this finding, we used transmission electron microscopy (TEM) to detect immunogold-labeled-STC1 (black dots), which shows binding on mitochondria (M, Fig. 6B). Compared with the study presented by McCudden *et al.*, in which they investigated the cellular location of STC1 with electron microscopy (24), we were able to minimize background binding and detect positive signals on mitochondria.

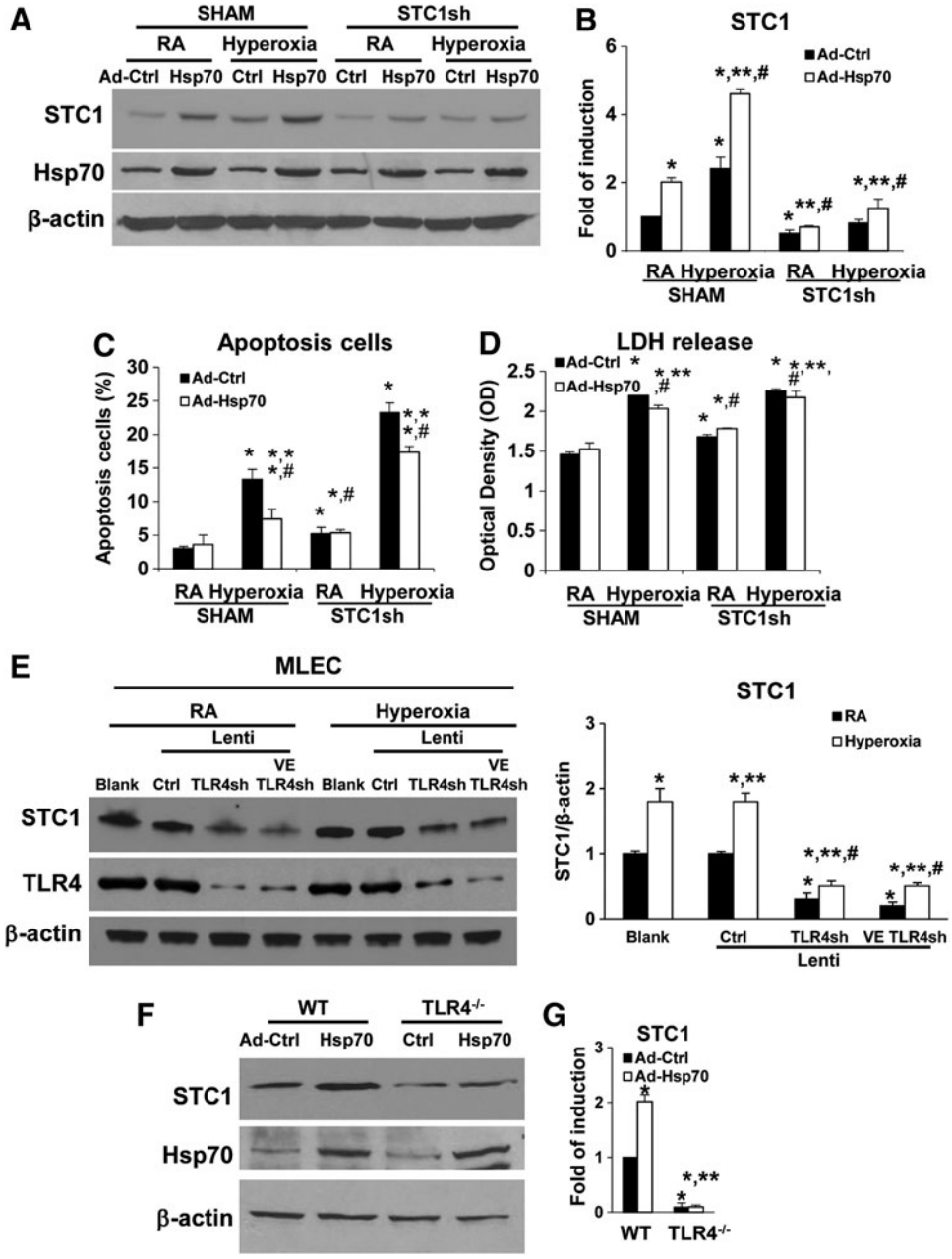

FIG. 4. Hsp70-TLR4 signal mediates STC1 induction. (A–D) WT MLECs were transfected with Ctrl shRNA (SHAM) or STC1 sh and treated with Ad-Ctrl or Ad-Hsp70 and exposed to 72 h of hyperoxia or RA as control. Uncut gel is shown in Supplementary Figure S9D. **(A)** Lysates were isolated and immunoblotted against STC1 and Hsp70 antibodies. β-Actin was used as protein loading control. **(B)** *STC1* mRNA expression was measured by real-time RT-PCR. Graphical quantitation of flow cytometry analysis of apoptosis, the mean ± SD was determined in **(C)**. The representative *dot plots* out of three experiments are shown in Supplementary Figure S6A. The LDH activity was determined in **(D)**. $^{*}p < 0.05$ *vs* SHAM Ctrl; $^{**}p < 0.05$ *vs* corresponding Ctrl; $^{\#}p < 0.05$ *vs* corresponding SHAM (experiments were performed in triplicates). **(E)** WT MLECs were treated with lentivirus (lenti-Ctrl, lenti-TLR4sh, or lenti-VE TLR4sh) and exposed to 72 h of hyperoxia or RA as control. Lysates were isolated and immunoblotted against STC1 and TLR4 antibodies. β-Actin was used as protein loading control. One representative Western blot of three experiments is shown. *Right panel*: quantification based on densitometry for STC1 relative to β-actin. The values are expressed as mean ± SD. Experiments were performed in triplicate $^{*}p < 0.05$ *vs* lenti-Ctrl RA; $^{**}p < 0.05$ *vs* corresponding RA, $^{\#}p < 0.05$ *vs* lenti-Ctrl hyperoxia. **(F, G)** WT and *TLR4*$^{-/-}$ MLECs were treated with Ad-Ctrl or Ad-Hsp70. **(F)** Lysates were isolated and immunoblotted against STC1 and Hsp70 antibodies. β-Actin was used as protein loading control. One representative Western blot of three experiments is shown. Uncut gel is shown in Supplementary Figure S9E. **(G)** *STC1* mRNA expression was measured by real-time RT-PCR. $^{*}p < 0.05$ *vs* WT Ad-Ctrl; $^{**}p < 0.05$ *vs* corresponding WT; $^{\#}p < 0.05$ *vs TLR4*$^{-/-}$ Ad-Ctrl or RA (experiments were performed in triplicates). Data were analyzed by two-way ANOVA with *post hoc* Tukey's HSD test calculator for multiple comparisons. Ad-Ctrl, adenovirus-control (CMV-null); Ad-Hsp70, adenoviral Hsp70; Hsp70-TLR4, heat shock protein 70–toll-like receptor 4; shRNA, short hairpin RNA.

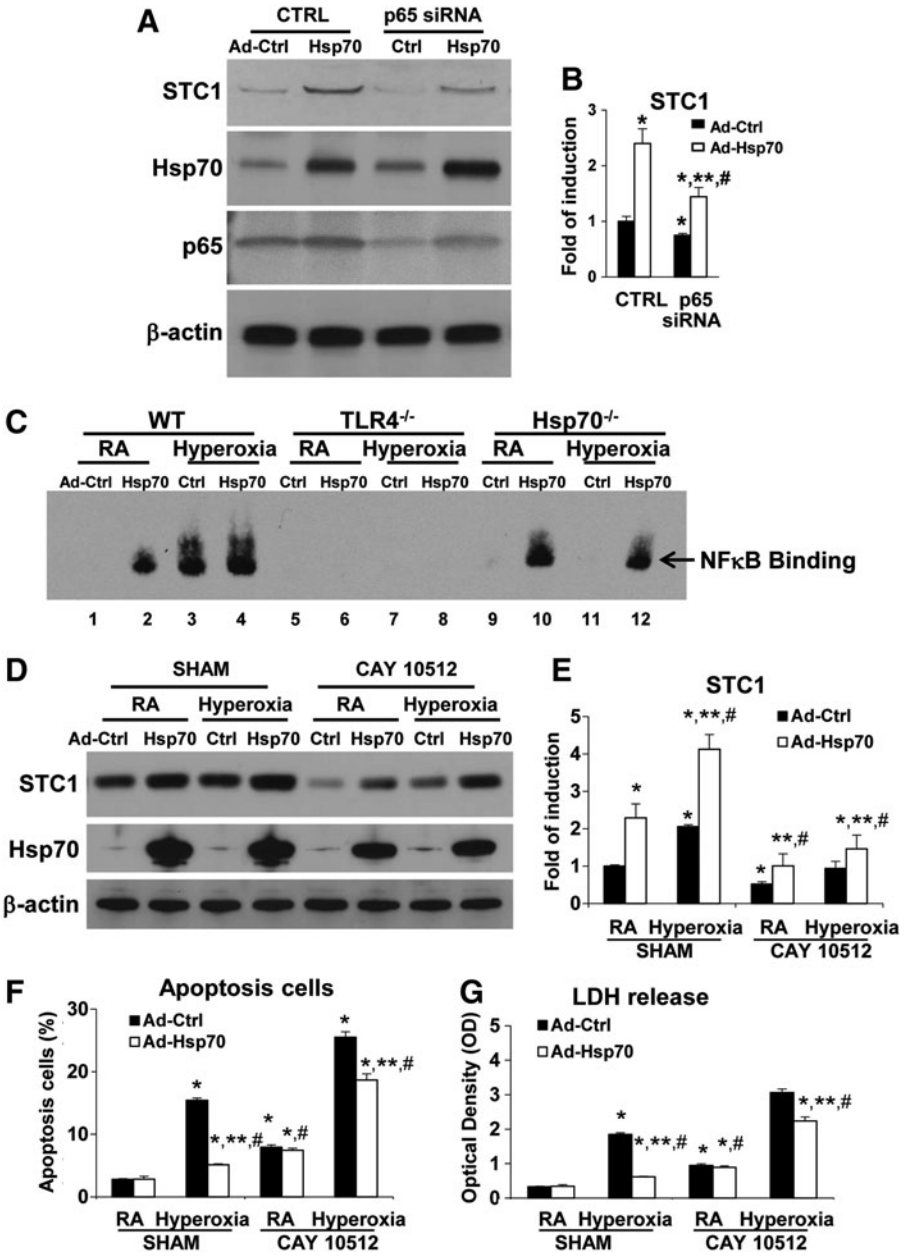

FIG. 5. Hsp70-TLR4-NFκB signal mediates STC1 induction and hyperoxic protection. WT MLECs were transfected with Ctrl siRNA or NFκB p65 siRNA and treated with Ad-Ctrl or Ad-Hsp70. **(A)** Lysates were isolated and immunoblotted against STC1, Hsp70, and p65 antibodies. β-Actin was used as protein loading control. Uncut gel is shown in Supplementary Figure S9F. **(B)** *STC1* mRNA expression was measured by real-time RT-PCR. $^{*}p<0.05$ *vs* Ctrl siRNA Ad-Ctrl; $^{**}p<0.05$ *vs* Ctrl siRNA Ad-Hsp70; $^{\#}p<0.05$ *vs* corresponding Ad-Ctrl. **(C)** Detection of NFκB DNA binding by EMSA. WT, *TLR4*$^{-/-}$, or *Hsp70*$^{-/-}$ MLECs were treated with Ad-Ctrl or Ad-Hsp70 and exposed to 72 h of hyperoxia or RA as control. Uncut gel is shown in Supplementary Fig. S10A. **(D–G)** WT MLECs treated with CAY10512 (NFκB inhibitor) 2 mg/mL for 1 h and treated with Ad-Ctrl or Ad-Hsp70 and exposed to 72 h of hyperoxia or RA as control. **(D)** Lysates were isolated and immunoblotted against STC1 and Hsp70 antibodies. β-Actin was used as protein loading control. Uncut gel is shown in Supplementary Figure S10B. **(E)** *STC1* mRNA expression was measured by real-time RT-PCR. Graphical quantitation of flow cytometry analysis of apoptosis, the mean ± SD was determined in **(F)**. The representative *dot plots* out of three experiments are shown in Supplementary Figure S6B. The LDH activity was determined in **(G)**. $^{*}p<0.05$ *vs* SHAM Ad-Ctrl; $^{**}p<0.05$ *vs* corresponding Ad-Ctrl; $^{\#}p<0.05$ *vs* corresponding SHAM (experiments were performed in triplicates). Data were analyzed by two-way ANOVA with *post hoc* Tukey's HSD test calculator for multiple comparisons. EMSA, electromobility shift assay; NF-κB, nuclear factor kappa-light-chain-enhancer of activated B cells; siRNA, small interfering RNA.

Moreover, we investigated the colocalization of STC1 and the mitochondrial marker Hsp60 in WT and *TLR4*$^{-/-}$ MLECs during room air (RA) and hyperoxic conditions. We confirmed that *TLR4*$^{-/-}$ MLECs have significantly decreased mitochondrial STC1, especially after hyperoxia (Fig. 6C). We quantified and normalized the fluorescence intensity of STC1 detection, as shown in the right panel of Figure 6C.

We were also able to knockdown basal mitochondrial STC1 in WT MLECs using lentiviral STC1 sh, whereas lentiviral STC1 overexpression (oe) restored mitochondrial STC1 in *TLR4*$^{-/-}$ MLECs (Fig. 7A). We quantified and normalized the fluorescence intensity of STC1 detection, as shown in the right panel of Figure 7A. STC1 has been reported to regulate calcium and plays a critical role in transendothelial migration of inflammatory cells at baseline and during inflammation (3). We used Rhod2-AM, a mitochondria Ca^{2+} level indicator, to investigate changes in calcium levels when we manipulated STC1 expression in MLECs. As shown in Figure 7B, *TLR4*$^{-/-}$ MLECs exhibited greater calcium in the mitochondria compared with WT MLECs, which was amplified after hyperoxia. Calcium levels increased in WT MLECs after STC1 knockdown by lenti-STC1shRNA, whereas the levels were decreased in *TLR4*$^{-/-}$ MLECs treated with STC1 overexpression using lenti-STC1oe.

We quantified mitochondrial calcium levels, as shown in the right panel of Figure 7B. STC1 expression correlated with changes in mitochondrial architecture in MLECs. Mitochondrial area and length were significantly higher in WT MLECs, a sign of healthy preserved mitochondria, whereas *TLR4*$^{-/-}$ MLECs had a greater number of swollen mitochondria with loss of normal architecture and distortion of cristae (Fig. 7C). We quantified the changes in cristae architecture, as shown in the right panel of Figure 7C. *TLR4*$^{-/-}$ MLECs had greater numbers of autolysosomes, a sign of increased turnover of organelles and proteins. WT MLECs with STC1 knockdown exhibited similar mitochondrial structural changes to that of *TLR4*$^{-/-}$ MLECs. The overexpression of STC1 in *TLR4*$^{-/-}$ MLECs restored the mitochondrial architecture to a normal appearance, similar to WT MLECs.

TLR4-STC1 promotes glycolysis

Glycolysis results in the breakdown of glucose into pyruvate/lactate. Pyruvate is converted to acetyl CoA, which acts as fuel for the citric acid cycle in the subsequent stages of cellular respiration. In eukaryotic cells, the citric acid cycle occurs in the matrix of the mitochondrion (29).

Trif and myeloid differentiation primary response gene 88 (MyD88) are the major downstream adaptor proteins for TLR4 signaling. We have previously reported that Hsp70-dependent TLR4 signaling requires Trif rather than the more commonly reported MyD88 pathway (45). In a glucose uptake assay, we found that *TLR4*$^{-/-}$ and *Trif*$^{-/-}$ MLECs had reduced 2-(*N*-(7-Nitrobenz-2-oxa-1,3-diazol-4-yl)Amino)-2-deoxyglucose (2-NBDG) uptake compared with WT MLECs. Using *Hsp70*$^{-/-}$ MLECs, we show that the loss of Hsp70 (which we had previously described as an endogenous TLR4 ligand in MLECs) also led to decreased uptake of 2-NBDG. *MyD88*$^{-/-}$ MLECs had relatively more 2-NBDG uptake compared with other knockout MLECs (Fig. 8A, B). We restored glucose uptake in *TLR4*$^{-/-}$ MLECs with lenti-STC1oe lentivirus. As shown in Figure 8C and D, the overexpression of STC1 increased glucose uptake in both WT and *TLR4*$^{-/-}$ MLECs.

We also measured glycolysis and found that *TLR4*$^{-/-}$ MLECs had decreased basal glycolysis and glycolytic capacity, which was restored with the overexpression of STC1 using lenti-STC1oe. Knockdown of STC1 with lenti-STC1sh decreased basal glycolysis and glycolytic capacity in WT MLECs (Fig. 8E). We confirmed that *TLR4*$^{-/-}$ MLECs had decreased basal and compensatory glycolysis, although the percentage of proton efflux rate (PER) from basal glycolysis was the same as that of WT MLECs, as measured by the glycolytic rate assay (Fig. 8F).

STC1 maintains cellular and mitochondrial bioenergetics

To understand the impact of STC1 on cellular and mitochondrial functions, especially in *TLR4*$^{-/-}$ MLECs, we measured the oxygen consumption rate (OCR) in *TLR4*$^{-/-}$ and WT MLECs using a Seahorse Biosciences extracellular flux analyzer. We observed higher OCR in WT compared with *TLR4*$^{-/-}$ MLECs (Fig. 9A). We analyzed mitochondrial bioenergetic measurements, including basal respiration, proton leak, ATP (adenosine triphosphate)-production-related oxygen consumption, maximum respiration, and coupling efficiency (10), all of which were significantly lower in *TLR4*$^{-/-}$ compared with WT (Fig. 9B, C). The data show lower oxygen demand in *TLR4*$^{-/-}$ with concomitantly lower production of ATP. ECAR (extracellular acidification rate), a measure of glycolysis (Fig. 8F), was also lower in *TLR4*$^{-/-}$ MLECs, which correlated with lower mitochondrial respiration (Fig. 9A–C).

FIG. 6. *TLR4*$^{-/-}$ MLECs have decreased mitochondrial STC1 during RA and hyperoxic conditions. (A) Colocalization of STC1 in MLECs. MLECs were immunostained for STC1 plus mitochondrial marker Hsp60, golgi marker Golgin-97, or endoplasmic reticulum marker ERp72. Nuclei were stained with DAPI (*blue*). *Left panel* shows single immunostained and merged images, original view of all photomicrographs × 1000. *Right panel* shows the quantification of colocalization; the fraction of STC1 that colocalizes with the cellular organelle markers is represented by the colocalization coefficient. $*p < 0.05$ *vs* STC1/mito. Data are representative of at least 20 images. **(B)** Immunogold labeling of STC1 protein in MLECs. WT MLECs were exposed to 72 h of hyperoxia or RA as control. Note: dense labeling (*black deposits*) over mitochondria observed with the transmission electron microscopy. M, mitochondria; *black arrows*, endoplasmic reticulum. Bar = 250 nm. **(C)** Immunostaining for STC1 (*red*) and Hsp60 (mitochondria marker, *green*) with DAPI-stained nuclei (*blue*) in WT or *TLR4*$^{-/-}$ MLECs was exposed to 72 h of hyperoxia or RA as control. *Left panel* shows single immunostained and merged images, original view of all photomicrographs × 1000. *Right panel* shows the normalized fluorescence of STC1 using the ImageJ software. $*p < 0.05$ *vs* WT RA; $**p < 0.05$ *vs* WT hyperoxia; $^{\#}p < 0.05$ *vs* *TLR4*$^{-/-}$ RA. Data are representative of at least 20 images. Data were analyzed by two-way ANOVA with *post hoc* Tukey's HSD test calculator for multiple comparisons. Color images are available online.

These results suggest a lower metabolic rate in *TLR4*$^{-/-}$ MLECs. The bioenergetics of *TLR4*$^{-/-}$ MLECs paralleled that of STC1 silencing in WT MLECs, whereas STC1 overexpression restored the bioenergetics of *TLR4*$^{-/-}$ MLECs to that of WT MLECs, suggesting that STC1 specifically regulates cellular and mitochondrial metabolic profiles and its effects appear to be mediated by TLR4 in MLECs (Fig. 9D–F). Interestingly, exogenous hSTC1 improved mitochondrial bioenergetics in both WT and *TLR4*$^{-/-}$ MLECs (Supplementary Fig. S7).

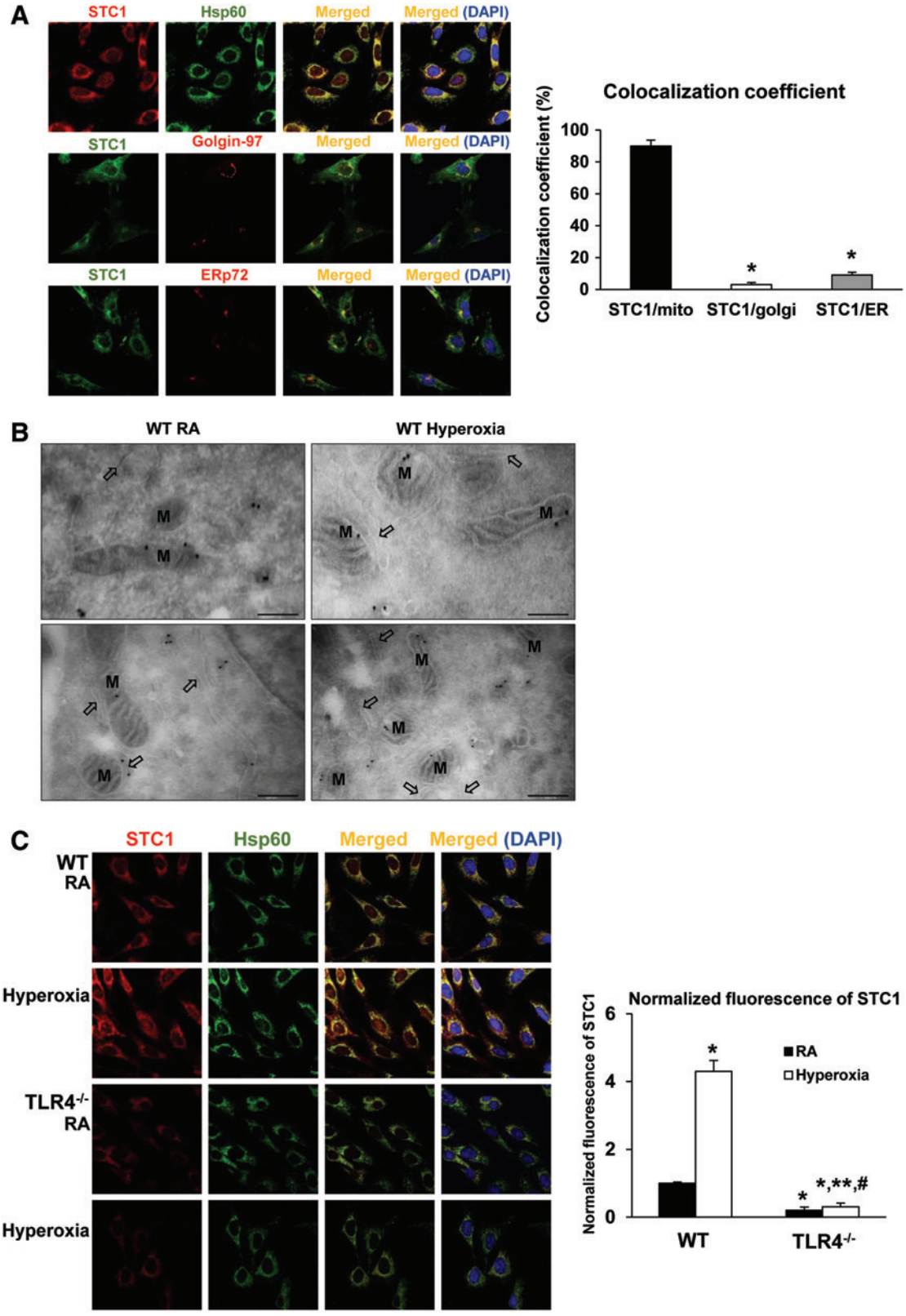

Loss of endothelial STC1 in vivo *increases mortality*

TLR4$^{-/-}$ mice lungs had less basal as well as hyperoxia-induced STC1 expression (Fig. 10A). To investigate whether Hsp70-TLR4-NFκB regulated STC1 expression *in vivo*, we treated WT mice with intranasal, and thus, lung-targeted, Ad-Ctrl or Ad-Hsp70 before 72 h of hyperoxia, a time point we previously found to reflect maximal lung injury. We confirmed that hyperoxia induced STC1 protein expression (Fig. 10B). Hsp70 overexpression, using Ad-Hsp70, also induced STC1 in WT mouse lungs.

We performed TLR4 overexpression experiments using lentiviral-driven human TLR4 constructs that target all lung cells or endothelium, lenti-hTLR4, and lenti-VE hTLR4, respectively. We found that all lung- or endothelial-targeted TLR4 overexpression induced both basal and hyperoxia-associated STC1 expression in WT lungs (Fig. 10C).

Given that STC1-knockout mice are not readily available to us, we performed *in vivo* loss-of-function experiments by designing all-cell and endothelium (Ec)-targeting STC1 silencing constructs (STC1shRNA or VE-STC1shRNA, respectively) and delivered them intranasally to WT mice, to achieve lung endothelial specificity, using our previously reported methods (14, 33, 42–44).

We first tested lung and cell specificity by creating single-cell lung suspensions from the lungs, using magnetic-activated cell sorting technology (Miltenyi Biotec), and cell selection with Ec (CD31) and non-Ec (CD45) cell markers after lentiviral delivery (Supplementary Fig. S8A). As expected, all-lung cell-targeting constructs (lenti-STC1shRNA) reduced *STC1* gene expression in total lung lysates, Ec, and other cell types, whereas Ec-targeting lentivirus (lenti-VE-STC1shRNA) targeted Ec and total lungs (given that Ec composes >40% of total lung cells, this effect on total lung expression is expected). These results confirmed our previous reports of all-lung and Ec-targeting using intranasal lentiviral constructs (14, 33, 42–44). Silencing STC1 specifically in Ec *in vivo* was sufficient to significantly shorten survival during HALI (Supplementary Fig. S8B).

Overexpression of STC1 protects against HALI in vivo

To demonstrate the impact of STC1 overexpression *in vivo*, we treated WT and *TLR4*$^{-/-}$ mice intranasally with lentivirus (lenti-Ctrl, STC1 overexpression lenti-STC1oe, or lenti-VE STC1oe) 2 weeks before 72 h hyperoxia. We confirmed the efficiency of these STC1 expression manipulations with protein detection, as shown in Supplementary Figure S8C. We found both lenti-STC1oe and lenti-VE STC1oe treatment significantly decreased lung permeability (bronchoalveolar lavage [BAL] cell counts, protein content, LDH, and oxidants) compared with lenti-Ctrl (Fig. 10D–G) in WT and *TLR4*$^{-/-}$ mice. Even *TLR4*$^{-/-}$ mice with endothelial STC1oe were much more resistant to lethal hyperoxia. Taken together, the results indicated that *in vivo* endothelial STC1 confers critical protective effects in WT and *TLR4*$^{-/-}$ mice during hyperoxia.

Discussion

Lung endothelial integrity and survival are critical determinants of the severity of lung injury. Oxidant stress causes endothelial cell injury, death, and, if unabated, organ failure. Excessive oxidant stress has been implicated in the pathogenesis of ALI or, its extreme form, acute respiratory distress syndrome (ARDS). Inhaled hyperoxia is a well-established model of experimental oxidant-induced ALI/ARDS. Mice exposed to hyperoxia exhibit pathophysiological changes characterized by endothelial as well as epithelial injury with inflammation and lung protein leak, resembling the features observed in clinical ALI/ARDS.

Identifying protective molecular pathways in hyperoxic lung injury may generate insights into novel therapeutic approaches. Our recent report found that the antioxidant functions of the innate immune receptor TLR4 depend on the presence of endothelial Hsp70. We now identify the downstream effector of Hsp70-TLR4-mediated protection, a putative antioxidant, STC1, which enriched in mitochondria of lung endothelium. Our studies show that STC1 is regulated by TLR4 and exerts lung and endothelial protection in response to sterile oxidant-induced lung injury.

Hyperoxia leads to an accumulation of mitochondrial dysfunction, increased ROS, and cell death (43). To detect ROS generation in the present study, we selected a variety of indirect but complementary assays. For example, CM-H2DCFDA primarily detects hydroxyl radical, peroxynitrite, and intracellular H_2O_2; Amplex Red detects extracellular H_2O_2; DHE detects cytosolic superoxide; and Mitosox Red detects mitochondrial superoxide. Mitochondrial ROS/superoxide generation can reflect mitochondrial dysfunction or

FIG. 7. STC1 expression correlated with changes in mitochondrial calcium loading and mitochondrial architecture in MLECs. WT MLECs were treated with lentivirus (lenti-Ctrl or lenti-STC1sh) and *TLR4*$^{-/-}$ MLECs were treated with lentivirus (lenti-Ctrl or STC1 overexpression lenti-STC1oe). **(A)** Immunostains for STC1 (*red*) and Hsp60 (mitochondria marker, *green*) with DAPI-stained nuclei (*blue*) in MLECs. *Left panel* shows single immunostained and merged images, original view of all photomicrographs × 400. *Right panel* shows the normalized fluorescence of STC1 using the ImageJ software. *$p < 0.05$ *vs* WT lenti-Ctrl; **$p < 0.05$ *vs* *TLR4*$^{-/-}$ lenti-Ctrl. Data are representative of at least 20 images. **(B)** MLECs were treated with lentivirus for 48 h followed by incubation with Rhod2-AM for 30 min. Cells were analyzed by fluorescence microscopy after Rhod2-AM staining (*red*). Nuclei were stained with DAPI (*blue*). *Left panel* shows the merged image as an overlay of the DAPI and Rhod2-AM images, original view of all photomicrographs × 1000. *Right panel* shows the quantification of the mitochondrial Ca^{2+}. *$p < 0.05$ *vs* WT lenti-Ctrl RA; **$p < 0.05$ *vs* WT lenti-Ctrl hyperoxia; $^{\#}p < 0.05$ *vs* corresponding RA. Data are representative of at least 20 images. **(C)** TEM was performed to investigate the ultrastructural differences in MLECs. M, mitochondria; *arrows* indicate endoplasmic reticulum; *indicates autolysosomes/amphisomes. Scale bar = 500 nm. *Right panel*: quantification of the mitochondrial width, the number of cristae per 500 nm of mitochondrial length, and the length of cristae mitochondrial ultrastructure organization. *$p < 0.05$ *vs* WT lenti-Ctrl; **$p < 0.05$ *vs* *TLR4*$^{-/-}$ lenti-Ctrl. Data are representative of at least 20 cells. Data were analyzed by two-way ANOVA with *post hoc* Tukey's HSD test calculator for multiple comparisons. TEM, transmission electron microscopy. Color images are available online.

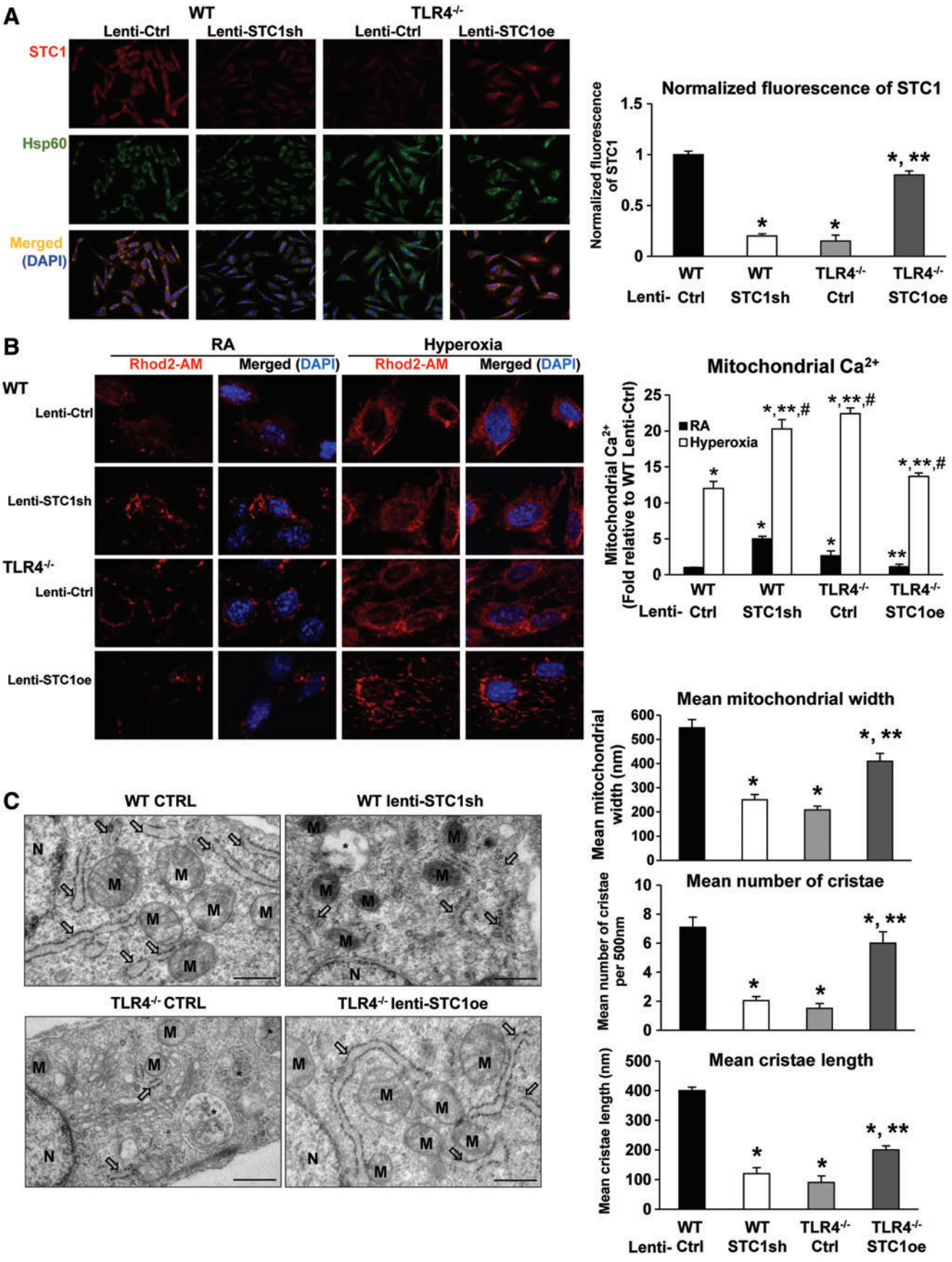
A
WT
TLR4-/-
Lenti-Ctrl
Lenti-STC1sh
Lenti-Ctrl
Lenti-STC1oe
STC1
Hsp60
Merged (DAPI)
Normalized fluorescence of STC1
Normalized fluorescence of STC1
1.5
1
0.5
0
*, **
*
*
WT Lenti- Ctrl
WT STC1sh
TLR4-/- Ctrl
TLR4-/- STC1oe
B
RA
Hyperoxia
Rhod2-AM
Merged (DAPI)
Rhod2-AM
Merged (DAPI)
WT
Lenti-Ctrl
Lenti-STC1sh
TLR4-/-
Lenti-Ctrl
Lenti-STC1oe
Mitochondrial Ca2+
Mitochondrial Ca2+ (Fold relative to WT Lenti-Ctrl)
25
20
15
10
5
0
RA
Hyperoxia
*
*,**,#
*
*,**,#
*
**
*,**,#
WT Lenti- Ctrl
WT STC1sh
TLR4-/- Ctrl
TLR4-/- STC1oe
C
WT CTRL
WT lenti-STC1sh
TLR4-/- CTRL
TLR4-/- lenti-STC1oe
N
M
Mean mitochondrial width
Mean mitochondrial width (nm)
600
500
400
300
200
100
0
*, **
*
*
Mean number of cristae
Mean number of cristae per 500nm
10
8
6
4
2
0
*, **
*
*
Mean cristae length
Mean cristae length (nm)
500
400
300
200
100
0
*, **
*
*
WT Lenti- Ctrl
WT STC1sh
TLR4-/- Ctrl
TLR4-/- STC1oe

health. We recently reported that hyperoxia, in normal lung endothelial cells, induced mitochondrial oxidant generation as well as inhibited mitophagy, autophagy, and mitochondrial biogenesis (42, 43).

Mitochondrial biogenesis refers to the growth and division of preexisting mitochondria, usually measured by the protein expression of PGC1α (22). Hyperoxia also disrupts the balance between mitochondrial fission and fusion in the lungs and MLECs (42). Das reported that hyperoxia increased mitochondrial ROS generation, which impairs mitochondrial electron transport chain function. He also revealed that hyperoxia decreased glycolytic capacity, glycolytic reserve, and oxidative phosphorylation and inhibits complex I and II function (6). We now identified STC1 and TLR4 as molecular targets, which may be manipulated to maintain or restore mitochondrial function.

STC1, originally called as teleocalcin, was first isolated from the corpuscles of Stannius of sockeye salmon (35). STC1 prevents excessive calcium influx to inside the fish body and protects organs and cells from high calcium levels that might cause cell death in fish (23). In mammals, the *STC1* gene is widely expressed in multiple tissues, including the adrenal grand, brain, heart, intestine, kidney, liver, lungs, muscle, ovary, pancreas, parathyroid, placenta, prostate, spleen, testis, thymus, and thyroid (26). STC1 has both autocrine and paracrine effects to maintain calcium homeostasis and to inhibit apoptosis. Its localization in the spleen and thymus suggests a role in the immune/inflammatory responses (30). STC1 promotes the re-epithelialization and cell migration during early wound healing in damaged tissues (38).

Upregulation and secretion of STC1 in mesenchymal stromal cells enhance cell survival by uncoupling oxidative respiration–phosphorylation, declining intracellular ROS, and switching metabolism toward a more glycolytic metabolic pattern (25). STC1 is thought to maintain endothelial permeability and prevent vascular leakage through the preservation of tight junction protein expression and suppression of superoxide anion production, thereby preserving the endothelial monolayer seal during cardiovascular inflammation (4). In macrophages, STC1 decreases intracellular calcium and cell mobility, attenuates the chemoattractants' responses, and decreases superoxide generation by UCP2 induction (30).

Pivotal work from McCudden *et al.* characterized mammalian STC receptors with receptor binding analysis, subsequent binding assays, *in situ* ligand binding, and fractionation analysis (24). They revealed that the majority of binding sites of STC were on the inner mitochondrial membrane and external cell membranes. They also revealed that >90% of cellular STC immunoreactivity were in the inner matrix of mitochondria with subcellular fractionation assay. Compared with the immunogold electron microscopy images in their study, we were able to optimize experimental conditions to minimize background binding, allowing us to more clearly detect positive signals for STC1 on mitochondria in lung endothelial cells.

We also performed TEM to observe ultrastructural changes in the mitochondria of MLECs with STC1 expression manipulation. Mitochondrial area and length are measures of dysfunction or health of mitochondria. In addition, TEM investigates organelle architectural changes such as mitochondrial fusion and fission. Mitochondria fusion connects neighboring mitochondria and merges their contents to maintain membrane potential. In contrast, fission separates damaged mitochondria from undamaged ones, where the damaged portion of mitochondria is subjected to mitophagy and the undamaged part to fusion. A fusion/fission imbalance can lead to accrual of dysfunctional or damaged mitochondria and subsequent degradation by autophagy.

Macroautophagy (autophagy) is a lysosomal-dependent cellular pathway for the turnover of organelles and proteins. Autophagy involves the formation of double membrane vesicles (autophagosomes or autophagic vacuoles) that target and engulf cytosolic material, which may include damaged organelles or denatured proteins. Based on the TEM results, we found that STC1 expression correlated with changes in mitochondrial architecture in MLECs. *TLR4*$^{-/-}$ MLECs had a

FIG. 8. TLR4-STC1 coordination promotes glycolysis. (A, B) WT, *TLR4*$^{-/-}$, *Trif*$^{-/-}$, *Myd88*$^{-/-}$, and *Hsp70*$^{-/-}$ MLECs were incubated with fluorescence-labeled glucose (100 μM 2-NBDG) for 30 min. Fluorescence was measured using a fluorescent microscope **(A)** or a fluorescence plate reader **(B)**. Original view of all photomicrographs × 400 in **(A)**. Values are expressed as means ± SD in **(B)**; experiments were performed in triplicate. *$p < 0.05$ *vs* WT. **(C, D)** WT and *TLR4*$^{-/-}$ MLECs were pretreated with lentivirus (lenti-Ctrl or lenti-STC1oe, STC1 overexpression) for 48 h followed by incubation with fluorescence-labeled glucose (100 μM 2-NBDG) for 30 min. Fluorescence was measured using a fluorescence plate reader **(C)** or analyzed by fluorescent microscope **(D)**. Values are expressed as means ± SD in **(C)**; experiments were performed in triplicate. *$p < 0.05$ *vs* WT lenti-Ctrl; **$p < 0.05$ *vs* *TLR4*$^{-/-}$ lenti-Ctrl; $^{\#}p < 0.05$ *vs* WT lenti-STC1oe. **(E, F)** WT MLECs were treated with lenti-Ctrl or lenti-STC1sh and *TLR4*$^{-/-}$ MLECs were treated with lenti-Ctrl or lentivirus with STC1 overexpression (lenti-STC1oe). **(E)** Glycolysis assays were performed using glycolysis test kits from Seahorse Biosciences according to manufacturer's protocol using XF96 instrument. A representative graph output from XF96 showing the ECAR response to glucose, oligomycin, and 2-DG in normoxia and calculating glycolysis. The minimum number of $n = 3$ with 10–20 replicate wells per group was employed for all experiments. Data normalized to 10,000 cells; *$p < 0.05$ *vs* WT lenti-Ctrl; **$p < 0.05$ *vs* *TLR4*$^{-/-}$ lenti-Ctrl. **(F)** Glycolytic rates were performed using glycolytic rate assay kit from Seahorse Biosciences according to manufacturer's protocol using XF96 instrument. The representative graph output for basal glycolysis, % PER from glycolysis (basal), and compensatory glycolysis was generated from the Seahorse XF glycolytic rate assay report generator. Data were adjusted with the CO_2 correction factor as 0.69 in MLEC determined with Agilent Seahorse XF CO_2 contribution factor protocol. The minimum number of $n = 3$ with 10–20 replicate wells per group was employed for all experiments. Data normalized to 5000 cells; *$p < 0.05$ *vs* WT lenti-Ctrl; **$p < 0.05$ *vs* *TLR4*$^{-/-}$ lenti-Ctrl. Data were analyzed by two-way ANOVA with *post hoc* Tukey's HSD test calculator for multiple comparisons. 2-NBDG, 2-(*N*-(7-Nitrobenz-2-oxa-1,3-diazol-4-yl)Amino)-2-deoxyglucose; ECAR, extracellular acidification rate; Myd88, myeloid differentiation primary response gene 88; PER, proton efflux rate; Trif, TIR-domain-containing adapterinducing interferon-β. Color images are available online.

greater number of swollen mitochondria with loss of normal architecture and distortion of cristae, and greater number of autolysosomes. WT MLECs with STC1 knockdown exhibited similar mitochondrial structural changes as that of *TLR4*$^{-/-}$ MLECs. The overexpression of STC1 in *TLR4*$^{-/-}$ MLECs restored the mitochondrial architecture to a normal appearance, similar to WT MLECs.

The promoter of human STC1 contains multiple NFκB p65 binding sites, as reported previously (13). Guo *et al.* found that NFκB p65 protein directly bound the human STC1 promoter region and regulated STC1 expression in human cervical cancer cells, CaSki. In the present study, we confirmed the extracellular Hsp70-mediated TLR4-NFκB signaling through NFκB binding assay. In addition, we used NFκB inhibitor, CAY 10512, to confirm that Hsp70 acts as a TLR4-dependent ligand and utilizes a NFκB-STC1 signal to promote lung endothelial survival during basal and hyperoxic conditions.

The mitochondria are the core machinery for cellular energy generation. Calcium regulates mitochondrial function and acts at several levels to stimulate ATP synthesis. Within physiological conditions, Ca^{2+} is beneficial for mitochondrial

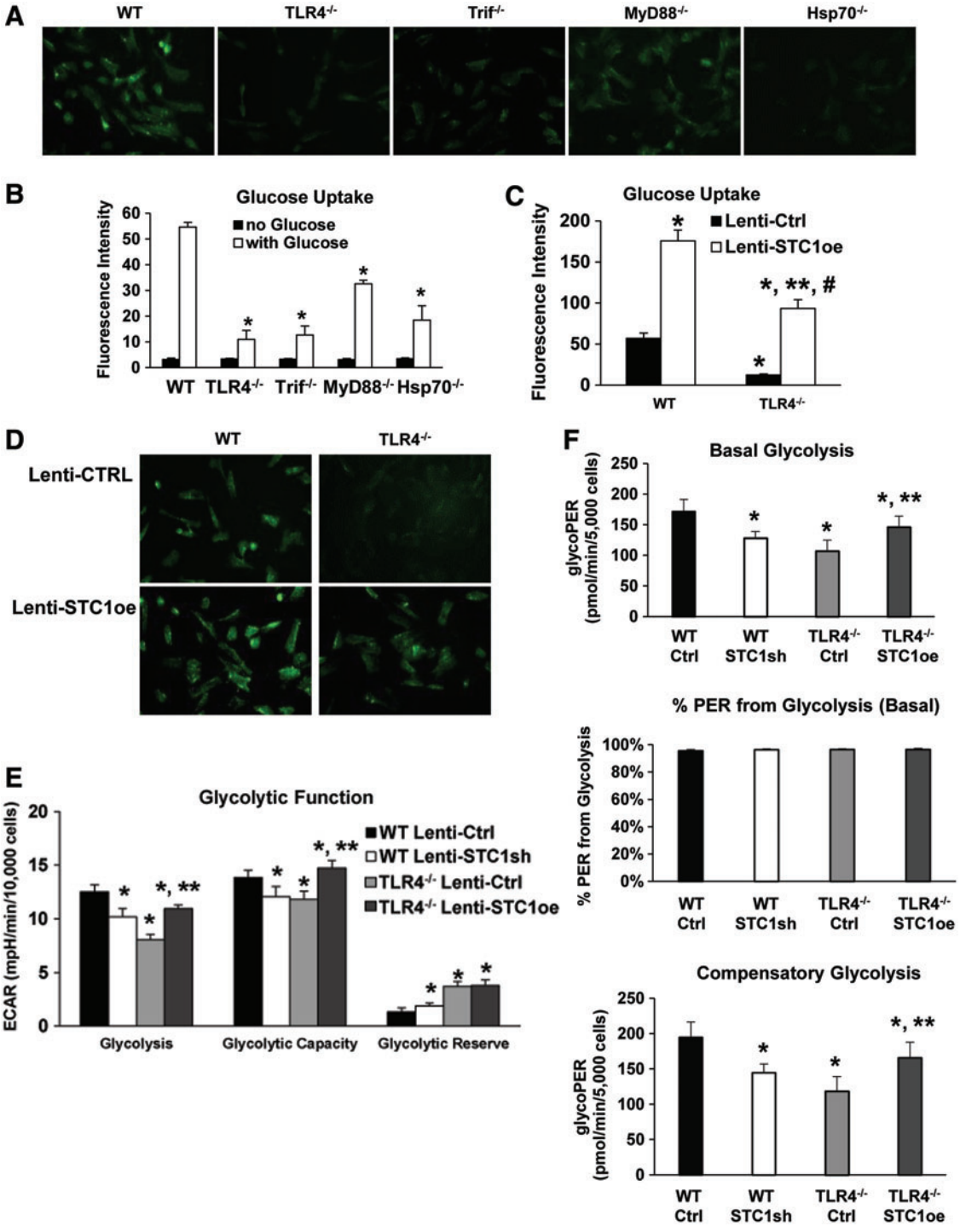

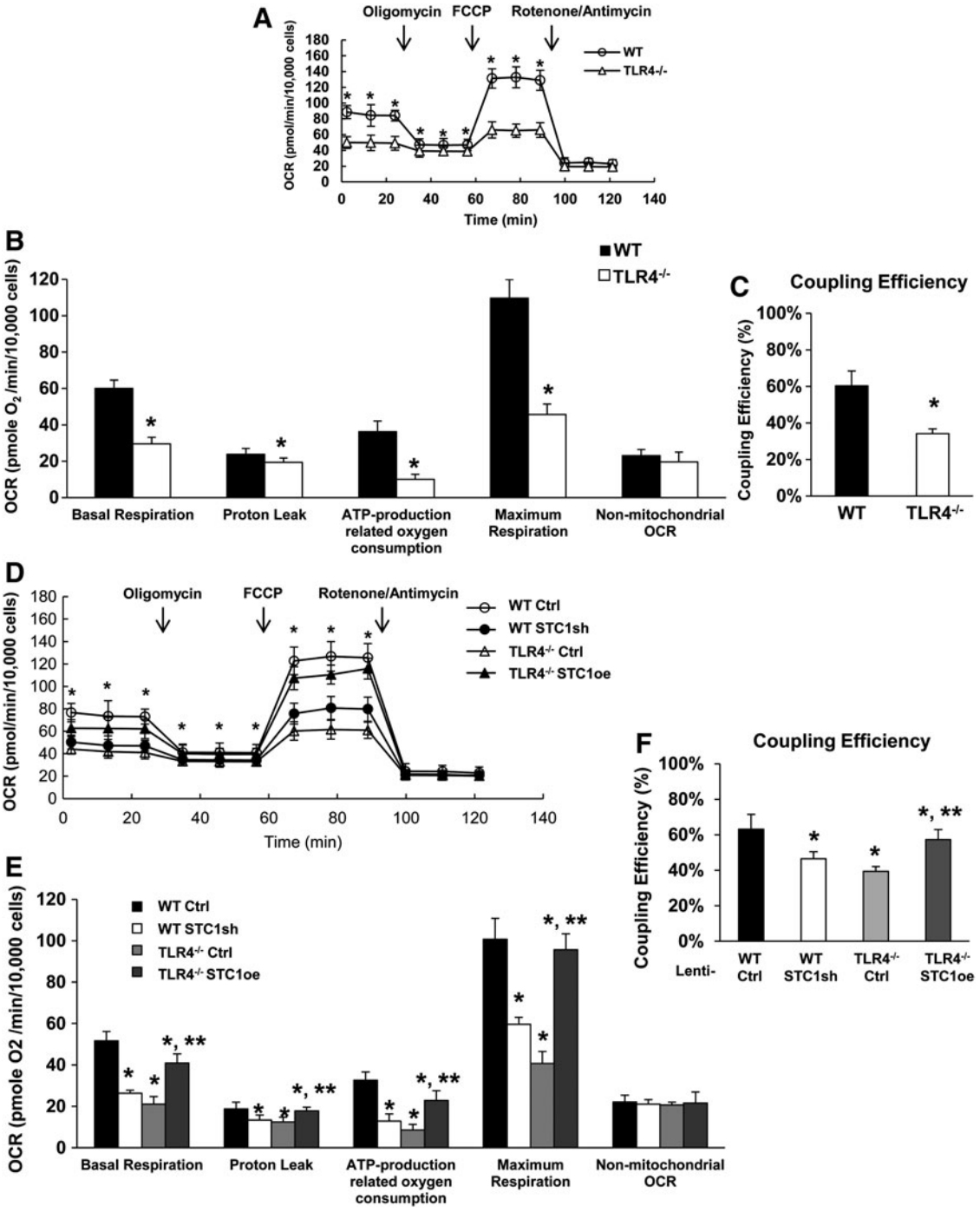

FIG. 9. STC1 maintains mitochondrial bioenergetics. **(A–C)** Comparison of mitochondrial function of WT and TLR4$^{-/-}$. **(A)** OCR was immediately measured using the Seahorse XF96 Analyzer. Kinetic OCR responses to oligomycin (1 μM), FCCP (5 μM), rotenone (1 μM), and antimycin (1 μM) were recorded. **(B)** Fundamental parameters of mitochondrial function including basal respiration, proton leak, ATP-production-related oxygen consumption, maximum respiration, and nonmitochondrial oxygen consumption rates were normalized based on number of live cells. **(C)** Mitochondrial coupling efficiency was calculated as the percentage of ATP production to basal mito-OCR (as ATP production/basal mito OCR × 100%). *$p < 0.05$ *vs* WT, $n = 10$–20. **(D–F)** WT MLECs were treated with lentivirus (lenti-Ctrl or lenti-STC1sh) and *TLR4*$^{-/-}$ MLECs were treated with lentivirus (lenti-Ctrl or STC1 overexpression lenti-STC1oe). Mitochondrial bioenergetic profile of MLECs was studied using the ''Mito stress kit,'' Seahorse Biosciences. **(D)** A representative graph output from XF96 showing the OCR response to oligomycin, FCCP, rotenone, and antimycin in normoxia. **(E)** Fundamental parameters of mitochondrial function including basal respiration, proton leak, ATP-production-related oxygen consumption, maximum respiration, and nonmitochondrial oxygen consumption rates were normalized based on number of live cells. **(F)** Mitochondrial coupling efficiency. A minimum number of $n = 3$ with 10–20 replicate wells per group was employed for all experiments. *$p < 0.05$ *vs* WT lenti-Ctrl; **$p < 0.05$ *vs* *TLR4*$^{-/-}$ lenti-Ctrl. Data were all normalized to 10,000 cells, using cell nuclei staining with Hoechst 33342 upon completion of Seahorse measurements. Real-time OCR were recorded and normalized with cell count using Wave Desktop 2.6. Data were analyzed by two-way ANOVA with Bonferroni's multiple comparisons test for pairwise comparisons in **(A)** and *post hoc* Tukey's HSD test calculator for multiple comparisons in **(B–F)**. ATP, adenosine triphosphate; FCCP, carbonyl cyanide-4-(trifluoromethoxy)phenylhydrazone; OCR, oxygen consumption rate.

function. The dysregulation of mitochondrial Ca^{2+} homeostasis plays a critical role in several pathologies. For instance, mitochondrial matrix Ca^{2+} overload might lead to enhanced ROS generation, triggering the permeability transition pore, and induced cytochrome *c* release, leading to apoptosis (2). The novel TLR4 antagonist, transforming growth factor-β-activated kinase-242, inhibited cytochrome *c* release into the cytoplasm, mitochondrial swelling, and decrease in mitochondrial Ca^{2+} buffering capacity (28).

As reported by Suliman *et al.*, TLR4 null mice have a disturbance in mitochondrial biogenesis during lipopolysaccharide challenge, due to the lack of NFκB-Creb1 activation of nuclear respiratory factor 1 (32). Ho *et al.* confirmed that an increase in mitochondria-associated calcium might decrease the efficiency of mitochondrial respiration, as a result of increased oxidative stress (15). STC1 regulates calcium/phosphate homeostasis and protects against toxic hypercalcemia. STC1 is a prosurvival factor that guards neurons against hypercalcemic and hypoxic damage (37). Ellard *et al.* also reported that STC1 stimulates mitochondrial electron transport chain activity and calcium transport (9). On the contrary, Guan *et al.* indicated that STC1-induced cardiotoxic effects might mediate mitochondrial dysfunction, loss of mitochondrial membrane potential, ROS production, and increased mitochondrial calcium levels (12).

STC1 was involved in the regulation of calcium level of endothelial function and plays a critical role in transendothelial migration of inflammatory cells at baseline and during inflammation (3). In the present study, we detected that *TLR4*$^{-/-}$ MLECs had more calcium uploading in the mitochondria compared with WT MLECs, which increased during hyperoxia exposure. The calcium level increased in WT MLECs after STC1 knockdown, whereas the calcium level decreased in *TLR4*$^{-/-}$ MLECs with STC1 overexpression. Although preliminary, these results suggest that STC1 may prevent mitochondrial calcium loading or uptake during hyperoxia-induced cell damage.

We currently lack precise methods to study glycoproteins in the lungs and have yet to identify a STC1 receptor. We used lentiviral approaches to achieve gain-of-function and loss-of-function to understand the STC1 biology, given our lack of access to STC1 knockout mice and cells, rather than as a therapeutic tool. However, we tested recombinant protein hSTC1, which decreased hyperoxia-induced oxidant production and ''normalized'' mitochondrial bioenergetics, which suggests that protein delivery may be a potential therapeutic approach in the clinic.

Most mammalian cells rely on glucose as one of the primary sources of energy to meet their bioenergetic needs. Through glycolysis, glucose is metabolized into pyruvate in the cytosol. Pyruvate can then either enter the tricarboxylic acid (TCA) cycle in the mitochondria, where it undergoes oxidative phosphorylation in a process that requires oxygen, or it can be further converted into lactate (anaerobic glycolysis) (34). Mice with a loss-of-function mutation in TLR4 (C3H/HeJ) were partially protected against cardiac glucose metabolism dysregulation induced by a long-term high-fat diet (20). TLR4 regulates lipid accumulation in cardiac muscle in type 1 diabetes, which contributes to cardiac dysfunction (7).

In the present study, we found that the *TLR4*$^{-/-}$ MLECs, TLR4 adaptor protein *Trif*$^{-/-}$, and TLR4 ligand *Hsp70*$^{-/-}$ MLECs had reduced glucose uptake compared with WT MLECs. The glycolysis assay showed that *TLR4*$^{-/-}$ MLECs had decreased basal glycolysis and glycolytic capacity, which was restored with the overexpression of STC1 using lenti-STC1oe. The glycolytic rate assay confirmed that *TLR4*$^{-/-}$ MLECs had decreased basal and compensatory glycolysis, although the percentage of PER from basal glycolysis was similar to that of WT MLECs. We interpreted these findings to indicate that Hsp70-TLR4-STC1 promotes cellular glycolysis.

We found STC1 to be predominantly expressed in endothelium in mouse lungs. There was some expression of STC1 around alveoli. TLR4-mediated STC1 expression likely affects most lung cell types, especially after hyperoxia. Reports have demonstrated the protective effects of STC1 in non-endothelial lung cell types. STC1 had antifibrotic effects through the reduction of oxidative stress, ER stress, and epithelial TGF-β1 production in bleomycin-induced idiopathic

FIG. 10. Lung endothelial STC1 is protective during hyperoxia. (A) WT and *TLR4*$^{-/-}$ mice were exposed to 72 h of hyperoxia or RA as control. Total lung lysates were immunoblotted against STC1 antibody. β-Actin was used as protein loading control. *Right panel*: quantification based on densitometry for STC1 relative to β-actin. The values are expressed as mean ± SD. Experiments were performed in triplicate $^{*}p < 0.05$ *vs* WT RA; $^{**}p < 0.05$ *vs* corresponding RA, $^{\#}p < 0.05$ *vs* WT hyperoxia. Uncut gel is shown in Supplementary Figure S10C. **(B)** WT mice were administered intranasal with Ad-Ctrl or Ad-Hsp70 and exposed to 72 h of hyperoxia or RA as control. Total lung lysates were immunoblotted against STC1 and Hsp70 antibodies. β-Actin was used as protein loading control. *Right panel*: quantification based on densitometry for STC1 relative to β-actin. The values are expressed as mean ± SD. Experiments were performed in triplicate $^{*}p < 0.05$ *vs* Ad-Ctrl RA; $^{**}p < 0.05$ *vs* Ad-Hsp70 RA, $^{\#}p < 0.05$ *vs* Ad-Ctrl hyperoxia. Uncut gel is shown in Supplementary Figure S11A. **(C)** WT mice were administered intranasal human TLR4 overexpressors, lentivirus (lenti-Ctrl, lenti hTLR4, or lenti-VE hTLR4), and exposed to 72 h of hyperoxia or RA as control. Lysates from mouse lungs were isolated and immunoblotted against STC1 antibody. β-Actin was used as protein loading control. One representative Western blot of three experiments is shown. *Right panel*: quantification based on densitometry for STC1 relative to β-actin. The values are expressed as mean ± SD. Experiments were performed in triplicate $^{*}p < 0.05$ *vs* lenti-Ctrl RA; $^{**}p < 0.05$ *vs* corresponding RA, $^{\#}p < 0.05$ *vs* lenti-Ctrl hyperoxia. **(D–G)** WT and *TLR4*$^{-/-}$ mice were administered intranasal lentivirus (lenti-Ctrl, STC1 overexpression lenti-STC1, or lenti-VE STC1) 2 weeks before exposed to 72 h of hyperoxia or RA as control. Cells recovered from BAL were counted as total cell counts **(D)**. **(E)** Lung permeability was assessed by BAL protein content. **(F)** The LDH activity assays were performed on BAL fluid. **(G)** Oxidant generation was detected by Amplex Red in BAL fluid. The values are expressed as mean ± SD ($n = 6$ for each group). $^{*}p < 0.05$ *vs* WT lenti-Ctrl RA; $^{**}p < 0.05$ *vs* WT lenti-Ctrl hyperoxia; $^{\#}p < 0.05$ *vs* corresponding RA; $^{\#\#}p < 0.05$ *vs TLR4*$^{-/-}$ Ctrl hyperoxia. Data were analyzed by two-way ANOVA with *post hoc* Tukey's HSD test calculator for multiple comparisons. BAL, bronchoalveolar lavage.

pulmonary fibrosis (27). STC1 was induced by hypoxia in both rat alveolar type II cells and human lung epithelial cells, reportedly promoting enhanced wound healing in alveolar epithelial cell monolayers (19). Our STC1 studies in lung endothelial cells raise intriguing possibilities as to its role in vascular biology.

In summary, we identified STC1 as a novel effector of Hsp70-TLR4 signaling and observed enriched STC1 expression in the mitochondria of normal lung endothelium. We confirmed that *TLR4*$^{-/-}$ mice and MLECs have significantly decreased mitochondrial STC1, especially after hyperoxia. At baseline, mitochondrial area and length were significantly

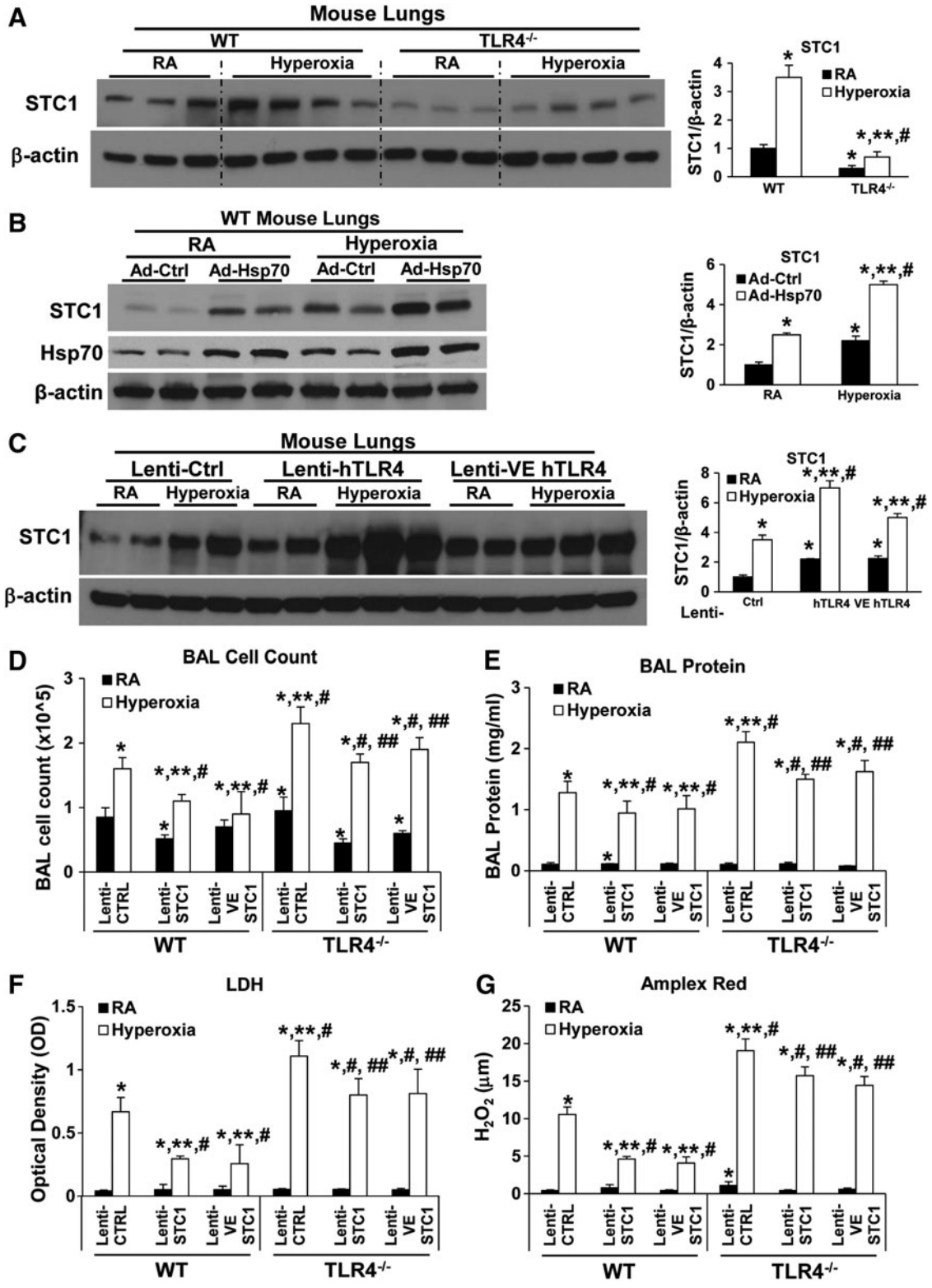

higher in WT MLECs, a sign of healthy preserved mitochondria, whereas *TLR4*$^{-/-}$ MLECs had greater numbers of swollen mitochondria with loss of normal architecture and distortion of cristae.

We found that TLR4 deficiency decreased the mitochondrial bioenergetic measurements (basal respiration, ATP-production-related oxygen consumption, and coupling efficiency). We detected higher mitochondrial calcium in *TLR4*$^{-/-}$ MLECs compared with WT MLECs, which was more pronounced after hyperoxia, suggesting dysregulated calcium metabolism in the absence of TLR4. STC1 silencing in WT MLECs phenocopied the mitochondrial dysfunction observed in *TLR4*$^{-/-}$ MLECs. STC1 overexpression in *TLR4*$^{-/-}$ MLECs rescued the mitochondrial morphology, calcium levels, glycolytic and mitochondrial profiles, and cellular respiration to that of WT levels. Finally, our *in vivo* loss-of-function and gain-of-function STC1 studies using lung and lung Ec-targeted lentiviral strategies demonstrated the therapeutic potential of STC1 targeting in ALI.

Materials and Methods

Mice

TLR4$^{-/-}$ mice (originally provided by Shizuo Akira, Osaka University, Osaka, Japan) have been previously described (40). *Hsp70*$^{-/-}$, *Trif*$^{-/-}$, and *MyD88*$^{-/-}$ mice were described previously (18, 45). All the mice were backcrossed for >10 generations onto a C57BL/6J background. Mice bred and exposed to hyperoxic conditions as described previously (42). All protocols were reviewed and approved by the Animal Care and Use Committee at the Yale University.

Hyperoxia exposures

Mice hyperoxia experiments and survival experiments had been described previously (31, 41, 44). Mice were placed in a Plexiglas chamber with 5 L/min of 100% oxygen continuous flow. Mice were allowed food and water *ad libitum*. In survival experiments, mice were monitored closely and their survival in hours was recorded. In injury experiments, after 72 h of hyperoxia exposure, mice were removed from the hyperoxia chamber and euthanized. All animal protocols were reviewed and approved by the Institutional Animal Care and Use Committee at the Yale University.

Measurement of lung injury markers

BAL and protein quantification have been described previously (42, 44). In brief, BAL was performed twice with 0.8 mL phosphate-buffered saline (PBS) (pH 7.4) when the mice were euthanized after 72 h of hyperoxia exposure or RA control. Cells in BAL were counted. The protein concentration was determined by the BCA Protein Assay Reagent (Thermo Fisher Scientific, Inc., Waltham, MA).

Isolation of primary MLECs and hyperoxia exposures

Isolation of MLECs from mouse lungs have been described previously (41, 44, 45). In brief, endothelial cells were isolated from the lungs of animals using anti-mouse CD31 antibody (clone MEC 13.3; BD Biosciences, San Jose, CA) and anti-mouse CD102 antibody (clone 3C4; BD Biosciences) bonded magnetic beads. For hyperoxia exposures, the cells were treated as described and subjected to hyperoxia (95% O_2 and 5% CO_2) for 72 h.

LDH assay

LDH was detected by Cytotoxicity Detection Kit (#11644793001; Roche, South San Francisco, CA) in the culture supernatant of MLECs and mouse BAL according to the manufacturer's instructions.

Amplex Red assay

Amplex® Red Hydrogen Peroxide/Peroxidase Assay Kit (A22188; Invitrogen, Carlsbad, CA) was used to check H_2O_2 released from mouse lung in BAL.

Microarray sample processing and hybridization

Total RNAs were isolated from primary WT or *TLR4*$^{-/-}$ MLECs and were subjected to amplification, followed by labeling and hybridization to Mouse Genome 430 2.0 GeneChip (Affymetrix, Santa Clara, CA) as described previously (45). In brief, total RNA was isolated using TRIzol reagent and further purified using an RNeasy kit (Qiagen, Valencia, CA). The quality of total RNA was evaluated by A_{260}/A_{280} ratio, which was at least 1.9, and by electrophoresis on the Agilent Bioanalyzer. For each experimental condition, 10 μg of high-quality total RNA was provided to the W.M. Keck Foundation Biotechnology Resource Laboratory at the Yale University (West Campus, Orange, CT). The facility performed the cRNA labeling, hybridization, and data analyses.

Microarray data processing

After scanning the array, the expression values for each gene were generated with the Affymetrix Microarray Suite (MAS) 5.0 software, scaling the overall intensity of each chip to 1500. All chips passed the Microarray Suite quality control measures. The individual gene expression levels of WT and TLR4$^{-/-}$ MLECs were compared by using an unpaired Student's *t* test. For further analyses, we selected 26 genes that met the following criteria: (i) $p < 0.001$ by unpaired *t* test; (ii) fold-change in expression of at least 1.5-fold between the mean expression in WT and the mean expression in TLR4$^{-/-}$ MLECs; and (iii) absolute difference of at least 200 signal units between the mean expression in WT and the mean expression in TLR4$^{-/-}$ MLECs. Multiple testing correction using the method of Benjamini–Hochberg was applied to the entire data set. The *p* values for these 26 genes remained significant ($p < 0.001$).

Construction of lentiviral vectors and administration

Lentivirus miRNA vectors with ubiquitin and vascular endothelium cadherin promoter had been described previously (42). STC1-knockdown vectors were designed using target site 1452–1473 (GenBank accession number NM_009285.3) 5′-ATTAGATGCAAGAAGATGCTAG-3′. We used Thermo Fisher Scientific, Inc., Scientific–Invitrogen's online RNAi Designer tool to design pre-miRNA stem loop/siRNA hybrid sequences according to the manufacturer's instructions. Two oligos, 5′-TGCTGATTAGATGCAAGAAGATGCTAGTTT TGGCCACTGACTGACTAGCATCTTTGCATCTAAT -3′ and 5′-CCTGATTAGATGCAAAGATGCTAGTCAGTCAG

TGGCCAAAACTAGCATCTTCTTGCATCTAATC-3′, were annealed and ligated into pcDNA6.2-GW/EGFP-miR (K493600; Thermo Fisher Scientific, Inc.) according to the manufacturer's instructions.

The constructs were confirmed by sequencing. The lentiviral constructs of EGFP-STC1-RNAi were constructed by first amplifying the fragments from pcDNA6.2-GW/EGFP-miR with primers, sense: 5′-AGGCGCGCCTGGCTAAC TAGAGAAC-3′ and antisense: 5′-GGAATTCTATCTCG AGTGCGGC-3′, and by digestion of the PCR product with *Asc*I and *EcoRI* enzymes. This fragment was then inserted into the *Asc*I and *Eco*RI sites of vectors FVEW or FUW (42) to generate lenti-VE STC1sh or lenti-STC1sh vectors. TLR4-knockdown vectors (lenti-TLR4sh and lenti-VE TLR4sh) were constructed using similar strategy and were designed using target site 550–570 (GenBank accession number NM_021297.2) 5′-GTACATGTGGATCTTTCTTAT-3′ (33).

Lentiviral STC1 overexpression (lenti-STC1oe or lenti-VE STC1oe) was constructed by amplifying the fragments from pCMV6 entry STC1 construct (STC1, [NM_009285] Mouse ORF Clone, MR203105, Origene, Rockville, MD) with primers, sense: 5′-AGGCGCGCCAATTCGTCGACTG GAT-3′ and antisense: 5′-GGAATTCGTTTAAACCTTAT CGTCGT-3′. The STC1 was recovered from the PCR fragment by *Asc*I and *Eco*RI digestion and then inserted into the *Asc*I and *Eco*RI sites of FVEW to generate lenti-VE STC1oe, or of FUW to generate lenti-STC1oe. All restriction endonucleases were purchased from New England Biolabs (Ipswich, MA). Lentivirus production, titer measurement, and intranasal administration were previously described (42). In lentivirus delivery experiments, 1×10^8 transduction units of the package lentiviral particles were administered intranasally to 6- to 8-week-old mice through a published intranasal method (42).

STC1 expression in endothelium modified with endothelial-targeting lentivirus

Endothelial cells ($CD31^+$, $CD45^-$) were isolated by the autoMACS system (Bergisch Gladbach, Germany) using manufacturer-supplied antibodies according to the manufacturer's instructions as described previously (44). RNA was isolated from each cell subfraction. For real-time PCR, the STC1 primers were used. GAPDH was amplified as a control.

Histology

Lungs sections were processed as described previously (44). In brief, 6–10 mice were analyzed in each experimental condition. Mouse whole lungs were fixed in buffered formalin at 4°C overnight, processed for paraffin embedding, and 5 μm sections were processed by the Yale Histopathology Services.

Immunofluorescence microscopy

The immunofluorescence was processed as described previously (44). For the co-staining, sections were incubated with a 1:200 dilution of anti-STC1 (sc-30183), anti-CD31 (sc-1506), anti-rat 10-kDa Clara cell promoter (CC10, sc-9773), anti-SP-C (sc-7705; Santa Cruz Biotechnology, Dallas, TX), or αSMA (ab7817; Abcam, Cambridge) antibody at 4°C for overnight. After PBS washes, sections were incubated with a secondary antibody Alexa Fluor 488 goat anti-rabbit IgG (A-11008) or Alexa Fluor 488 goat anti-mouse IgG (A-11001) or Alexa Fluor® 594 goat anti-rabbit IgG (A-11012; Invitrogen), with a 1:300 dilution for immunofluorescence at room temperature for 1 h.

Samples were washed three times by immersing in PBS for 5 min and then mounted with ProLong gold-mounting media with 4′,6-diamidino-2-phenylinodole (DAPI) (P36931; Thermo Fisher Scientific, Inc.). Labeled sections were observed under dark field in independent fluorescence channels using an automated Olympus BX-61 microscope (320 and 340 objective lens; NA 0.50; Olympus Imaging America, Inc., Center Valley, PA) equipped with a cooled CCD camera (Q-Color 5; Olympus) and QCapture Pro 6.0 software (QImaging; Surrey, Canada). Images were analyzed and quantified using the ImageJ software* (8). Data are representative of at least 20 images.

Confocal microscopy

MLECs were processed for confocal microscopy as described previously (45). Co-stained with anti-STC1 (sc-30183), Hsp60 (sc-1722; Santa Cruz Biotechnology), anti-Golgin-97 (#13192), or ERp72 (5033S; Cell Signaling Technology, Danvers, MA) at 4°C overnight. The secondary antibody (Alexa Fluor 488 goat anti-rabbit IgG or Alexa Fluor 594 goat anti-mouse IgG at 1:300 dilution; Invitrogen) was incubated at room temperature for 1 h. Labeled cells were visualized using a Nikon Ti-E Eclipse inverted microscope equipped with Perfect Focus (auto focus system), a motorized XY stage, and a Nano-Focusing Piezo Stage. Images were analyzed using the ImageJ software, and the colocalization coefficient was calculated to measure the fraction of overlapping signals using Coloc 2 (Fiji's plugin for colocalization analysis) (8).

Glucose uptake assay

MLECs were plated onto 24-well plates. After specific exposure as mentioned, the cells were added 100 μM 2-NBDG (N13195; Thermo Fisher Scientific, Inc.) and incubated for 30 min. Cells were washed twice with ice-cold PBS, and fluorescence was measured using a fluorescence plate reader for quantification. As well as to visualize the fluorescence after 2-NBDG uptake, the cells were fixed with ice-cold 4% PFA for 10 min at room temperature and analyzed by fluorescent microscope.

Mitochondrial calcium measurement and fluorescence staining

Rhod2-AM (R1244; Thermo Fisher Scientific, Inc.) was used to measure the mitochondrial calcium level as described previously (1). MLECs were grown on poly-L-lysine-coated coverslips (BD Biosciences). After specific exposure as mentioned, cells were stained with 7.5 μM Rhod2-AM in the culture medium for 2 h. Cells were fixed by incubation for 15 min at 4°C in 4% paraformaldehyde. Cells were washed in PBS, and images were acquired with Nikon Ti-E Eclipse inverted confocal microscope. Images were analyzed using the ImageJ software, and the quantification of mitochondrial

*http://imagej.nih.gov/ij/

Ca^{2+} was calculated to measure the fraction of Rhod2-AM signals (8).

Western blot analysis

Lung or MLEC protein analyses were performed as previously described (42). In brief, whole-lung tissues or MLECs were homogenized in M-PER™ mammalian protein extraction reagent (78501; Thermo Fisher Scientific, Inc.). Protein concentrations were determined by BCA Protein Assay (Thermo Fisher Scientific, Inc.). Samples were electrophoresed in a 4%–20% ready-made Tris-HCl gel (Bio-Rad Laboratories) and electrophoretically transferred onto a nitrocellulose membrane. The membranes were then incubated overnight with anti-STC1 (sc-30183), TLR4 (sc-293072), β-actin (sc-47778 HRP; Santa Cruz Biotechnology), p65 (#8242; Cell Signaling Technology, Inc.), and Hsp70 (ADI-SPA-812; Enzo Life Sciences, Inc., Farmingdale, NY) antibodies.

Apoptosis assays

A fluorescence-activated cell sorter (FACS) was used to detect Annexin V-fluorescein isothiocyanate labeling (#556547; BD Biosciences) on MLECs, as described previously (39, 44). Briefly, MLECs were resuspended with binding buffer (BD Biosciences); 5 μL each of Annexin V and propidium iodide were added to 10^5 cells. Cells were analyzed by FACS (BD Biosciences). Data were analyzed using the Flowjo software.

Flow cytometry assays for ROS

CM-H2DCFDA (C6827) and MitoSOX Red (M36008; Invitrogen) were used to determine the levels of ROS in endothelial cells, as described previously (44).

DHE staining and fluorescence microscopy

MLECs were adjusted to a density of 1×10^5 cells/mL and seeded on poly-L-lysine-coated coverslips (BD Biosciences) in a volume of 200 μL (2×10^4 cells). After treated with STC1 recombinant protein (100 ng/mL, MBS1265316; MyBioSource, San Diego, CA) for overnight, live cells were subjected to 2 μM DHE (D1168; Thermo Fisher Scientific, Inc.) as described previously (44).

Protein labeling

Recombinant protein was labeled with Alexa Fluor 488 dye, as described previously (45), by using the fluorescent Protein Microscale Labeling kit (A30006; Invitrogen) according to the manufacturer's recommendations. Briefly, 100 mg hSTC1 was incubated with Alexa Fluor 488 for 15 min at room temperature. Unconjugated dye was removed by using the spin filter. MLECs were transduced with CellLight™ Mitochondria-RFP, BacMam 2.0 (C10601; Invitrogen) at 20 particles per cell overnight to label mitochondria with red fluorescent protein in live cells.

Overexpression of Hsp70 in MLECs and mice

Adenovirus-CMV-Hsp70 (Ad-Hsp70) was purchased from Vector BioLabs. Adenovirus-control (CMV-null) (Ad-Ctrl), an adenovirus empty vector, was used as a control. The treatment to MLECs and mice had been described previously (45).

NFκB inhibitor

NFκB inhibitor, CAY10512, was purchased from Cayman Chemical (Ann Arbor, MI).

Transfection of siRNA duplexes

Mouse NFκB p65 siRNA (sc-29411) was purchased from Santa Cruz Biotechnology, Inc. Nonspecific siRNA scrambled duplex probes and transfection with Lipofectamine Reagent (Invitrogen) were used in MLECs, as described previously (40, 42).

Total RNA isolation and real-time reverse transcription–PCR amplification

Total RNA extracted from lung tissue or MLECs and real-time PCR amplification were described previously (42, 44). For real-time PCR, the STC1 primers were sense 5′-GTC CGAAGCCTTCTGGAATGT-3′ and antisense 5′-GGCTCA TTTGTACGCCTCCTAT-3′. GAPDH primers were sense 5′-TGTGTCCGTCGTGGATCTGA-3′ and antisense 5′-CC TGCTTCACCACCTTCTTGAT-3′. The primers were designed as intron spanning.

Electromobility shift assay

EMSAs of nuclear protein isolated from MLECs were performed as previously described (44, 45). In brief, nuclear extracts were prepared with NE-PER Nuclear Extraction Reagent Kit (Thermo Scientific). The sequence of NFκB consensus oligonucleotides was 5′-AGTTGAGGGGACTT TCCCAGGC-3′ (Santa Cruz Biotechnology). The nuclear extracts were biotin-labeled using double-stranded probes. EMSA was carried out using the LightShift Chemiluminescent EMSA Kit (Thermo Scientific). Specific binding was confirmed with 200-fold excess of unlabeled probe. Protein–DNA complexes were separated with a 6% nondenaturing acrylamide gel electrophoresis. The gel was transferred to positively charged nylon membranes and cross-linked with UV irradiation. Gel shifts were visualized with streptavidin horseradish peroxidase according to the manufacturer's protocol.

Measurement of mitochondrial bioenergetics

An XFe96 Analyzer (Agilent Technologies, Santa Clara, CA) was used to measure the bioenergetic function in intact MLECs in real time. After specific exposure as mentioned, MLECs in equal numbers were seeded into Seahorse Bioscience XFe96 cell culture plates at the seeding density of 10,000 cells in 80 μL media and allowed to adhere and grow for 24 h in a 37°C humidified incubator with 5% CO_2. Measurements of extracellular flux were made in unbuffered media. Mitochondrial function was analyzed by sequentially adding pharmacological inhibitors of oxidative phosphorylation, namely oligomycin (1 μM), FCCP [carbonyl cyanide-4-(trifluoromethoxy)phenylhydrazone] (5 μM), rotenone (1 μM), and antimycin (1 μM) (Sigma–Aldrich, St. Louis, MO).

The resultant bioenergetic profile provides detailed information on various parameters of mitochondrial bioenergetic components. Glycolysis assay was performed using glycolysis test kit from Agilent Technologies according to

manufacturer's protocol using XFe96 instrument. A representative graph output from XFe96 showing the ECAR response to glucose, oligomycin, and 2-DG in normoxia and calculating glycolysis. Glycolytic rate was performed using the glycolytic rate assay kit from Agilent Technologies and was analyzed by sequentially adding pharmacological inhibitors of oxidative phosphorylation, namely rotenone/antimycin A (0.5 μM) and 2-DG (50 mM).

The CO_2 correction factor was confirmed in both WT and TLR4$^{-/-}$ MLECs before performing the glycolytic rate assay according to the Agilent Seahorse XF CO_2 contribution factor protocol. Cell nuclei were stained using Hoechst 33342 (62249; Thermo Scientific) upon completion of the Seahorse procedure. Real-time ECAR and OCR were recorded and normalized to the cell nuclei count using Wave Desktop 2.6. The Seahorse XF Glycolytic Rate assay report-generator was used to analyze and generate the graphs.

Transmission electron microscopy

MLECs were fixed in 2.5% glutaraldehyde in 0.1 *M* cacodylate buffer (pH 7.4) and then post-fixed in 1% OsO_4 in the same buffer at room temperature for 1 h. After stained en bloc with 2% aqueous uranyl acetate for 30 min, cells were dehydrated in a graded series of ethanol to 100% and finally embedded in EMbed 812 resin. Blocks were then polymerized in 60°C oven for 24 h. Thin sections (60 nm) were cut by a Leica ultramicrotome and poststained with 2% uranyl acetate and lead citrate. Sample grids were examined with a FEI Tecnai transmission electron microscope at 80 kV of accelerating voltage; digital images were recorded with an Olympus Morada CCD camera and iTEM imaging software. TEM analysis was performed by the Electron Microscopy Core Facility in the Center for Cellular and Molecular Imaging (CCMI) at the Yale Medical School. Quantification of the mitochondrial width, the number of cristae per 500 nm of mitochondrial length, and the length of cristae mitochondrial ultrastructure organization were obtained using the ImageJ software (21).

Immunogold labeling of STC1

MLECs were fixed in a mixture of 2% paraformaldehyde and 0.1% glutaraldehyde in 0.1 *M* phosphate buffer (pH 7.4), sucrose protected, and plunge frozen in liquid nitrogen. The frozen sections (60 nm) were cut with a Leica cryoultramicrotome, sections were labeled with STC1 antibody (sc-30183; Santa Cruz), then with secondary antibody conjugated to 10 nm protein A-gold particles, and immunolabeled sections were examined with a FEI Tecnai BioTwin electron microscope that is equipped with a Morada CCD camera (Olympus). TEM analysis was performed by Electron Microscopy Core Facility in the CCMI at the Yale Medical School.

Statistics

Statistical analyses of data were conducted with two-way analysis of variance. Bonferroni's multiple comparisons test was used for pairwise comparisons. The Tukey honestly significant difference *post hoc* test calculator was applied to the multiple comparisons. The one factor comparison was analyzed by the Mann–Whitney test. Data are expressed as mean ± standard deviation. Significant difference was accepted at $p < 0.05$. Survival curves were produced with the Prism software (GraphPad, San Diego, CA). Statistical comparisons for survival curves were performed with the log-rank (Mantel-Cox) test. Affymetrix microarray data are expressed as mean fold change and p values; the data processing, normalization, and statistical analyses were described in the Microarray data processing section.

Acknowledgments

We thank Dr. Xinran Nick Liu (Electron Microscopy Core Facility in the CCMI at the Yale Medical School) for assistance with the TEM. We thank Dr. Tej K. Pandita for the original *Hsp70*$^{-/-}$ mice and Dr. Shizuo Akira for the original *TLR4*$^{-/-}$ mice. This work was supported by VAORD 118 58595, Department of Defense PR150809, FAMRI 150074, and R01 HL138396 to P.J.L.

Author Disclosure Statement

No competing financial interests exist.

References

1. Brisac C, Téoulé F, Autret A, Pelletier I, Colbère-Garapin F, Brenner C, Lemaire C, and Blondel B. Calcium flux between the endoplasmic reticulum and mitochondrion contributes to poliovirus-induced apoptosis. *J Virol* 84: 12226–12235, 2010.
2. Brookes PS, Yoon Y, Robotham JL, Anders MW, and Sheu SS. Calcium, ATP, and ROS: a mitochondrial love–hate triangle. *Am J Physiol Cell Physiol* 287: C817–C833, 2004.
3. Chakraborty A, Brooks H, Zhang P, Smith W, McReynolds MR, Hoying JB, Bick R, Truong L, Poindexter B, Lan H, Elbjeirami W, and Sheikh-Hamad D. Stanniocalcin-1 regulates endothelial gene expression and modulates transendothelial migration of leukocytes. *Am J Physiol Ren Physiol* 292: F895–F904, 2007.
4. Chen C, Jamaluddin MS, Yan S, Sheikh-Hamad D, and Yao Q. Human stanniocalcin-1 blocks TNF-alpha-induced monolayer permeability in human coronary artery endothelial cells. *Arterioscler Thromb Vasc Biol* 28: 906–912, 2008.
5. Cordeiro JV and Jacinto A. The role of transcription-independent damage signals in the initiation of epithelial wound healing. *Nat Rev Mol Cell Biol* 14: 249–262, 2013.
6. Das KC. Hyperoxia decreases glycolytic capacity, glycolytic reserve and oxidative phosphorylation in MLE-12 cells and inhibits complex I and II function, but not complex IV in isolated mouse lung mitochondria. *PLoS One* 8: e73358, 2013.
7. Dong B, Qi D, Yang L, Huang Y, Xiao X, Tai N, Wen L, and Wong FS. TLR4 regulates cardiac lipid accumulation and diabetic heart disease in the nonobese diabetic mouse model of type 1 diabetes. *Am J Physiol Heart Circ Physiol* 303: H732–H742, 2012.
8. Dunn KW, Kamocka MM, and McDonald JH. A practical guide to evaluating colocalization in biological microscopy. *Am J Physiol Cell Physiol* 300: C723–C742, 2011.
9. Ellard JP, McCudden CR, Tanega C, James KA, Ratkovic S, Staples JF, and Wagner GF. The respiratory effects of stanniocalcin-1 (STC-1) on intact mitochondria and cells: STC-1 uncouples oxidative phosphorylation and its actions are modulated by nucleotide triphosphates. *Mol Cell Endocrinol* 264: 90–101, 2007.
10. Ferrick DA, Neilson A, and Beeson C. Advances in measuring cellular bioenergetics using extracellular flux. *Drug Discov Today* 13: 268–274, 2008.

11. Filvaroff EH, Guillet S, Zlot C, Bao M, Ingle G, Steinmetz H, Hoeffel J, Bunting S, Ross J, Carano RA, Powell-Braxton L, Wagner GF, Eckert R, Gerritsen ME, and French DM. Stanniocalcin 1 alters muscle and bone structure and function in transgenic mice. *Endocrinology* 143: 3681–3690, 2002.
12. Guan J, Mishra S, Shi J, Plovie E, Qiu Y, Cao X, Gianni D, Jiang B, Del Monte F, Connors LH, Seldin DC, Lavatelli F, Rognoni P, Palladini G, Merlini G, Falk RH, Semigran MJ, Dec GW, Jr, Macrae CA, and Liao R. Stanniocalcin1 is a key mediator of amyloidogenic light chain induced cardiotoxicity. *Basic Res Cardiol* 108: 378, 2013.
13. Guo F, Li Y, Wang J, Li Y, Li Y, and Li G. Stanniocalcin1 (STC1) inhibits cell proliferation and invasion of cervical cancer cells. *PLoS One* 8: e53989, 2013.
14. Haslip M, Dostanic I, Huang Y, Zhang Y, Russell KS, Jurczak MJ, Mannam P, Giordano F, Erzurum SC, and Lee PJ. Endothelial uncoupling protein 2 regulates mitophagy and pulmonary hypertension during intermittent hypoxia. *Arterioscler Thromb Vasc Biol* 35: 1166–1178, 2015.
15. Ho YS, Xiong Y, Ma W, Spector A, and Ho DS. Mice lacking catalase develop normally but show differential sensitivity to oxidant tissue injury. *J Biol Chem* 279: 32804–32812, 2004.
16. Huang L, Belousova T, Chen M, DiMattia G, Liu D, and Sheikh-Hamad D. Overexpression of stanniocalcin-1 inhibits reactive oxygen species and renal ischemia/reperfusion injury in mice. *Kidney Int* 82: 867–877, 2012.
17. Huang L, Belousova T, Pan JS, Du J, Ju H, Lu L, Zhang P, Truong LD, Nuotio-Antar A, and Sheikh-Hamad D. AKI after conditional and kidney-specific knockdown of stanniocalcin-1. *J Am Soc Nephrol* 25: 2303–2315, 2014.
18. Hunt CR, Dix DJ, Sharma GG, Pandita RK, Gupta A, Funk M, and Pandita TK. Genomic instability and enhanced radiosensitivity in Hsp70.1- and Hsp70.3-deficient mice. *Mol Cell Biol* 24: 899–911, 2004.
19. Ito Y, Zemans R, Correll K, Yang IV, Ahmad A, Gao B, and Mason RJ. Stanniocalcin-1 is induced by hypoxia inducible factor in rat alveolar epithelial cells. *Biochem Biophys Res Commun* 452: 1091–1097, 2014.
20. Jackson EE, Rendina-Ruedy E, Smith BJ, and Lacombe VA. Loss of toll-like receptor 4 function partially protects against peripheral and cardiac glucose metabolic derangements during a long-term high-fat diet. *PLoS One* 10: e0142077, 2015.
21. Janer A, Prudent J, Paupe V, Fahiminiya S, Majewski J, Sgarioto N, Des Rosiers C, Forest A, Lin ZY, Gingras AC, Mitchell G, McBride HM, and Shoubridge EA. SLC25A46 is required for mitochondrial lipid homeostasis and cristae maintenance and is responsible for Leigh syndrome. *EMBO Mol Med* 8: 1019–1038, 2016.
22. Jornayvaz FR and Shulman GI. Regulation of mitochondrial biogenesis. *Essays Biochem* 47: 69–84, 2010.
23. Lafeber FP, Flik G, Wendelaar Bonga SE, and Perry SF. Hypocalcin from Stannius corpuscles inhibits gill calcium uptake in trout. *Am J Physiol* 254: R891–R896, 1988.
24. McCudden CR, James KA, Hasilo C, and Wagner GF. Characterization of mammalian stanniocalcin receptors. Mitochondrial targeting of ligand and receptor for regulation of cellular metabolism. *J Biol Chem* 277: 45249–45258, 2002.
25. Ohkouchi S, Block GJ, Katsha AM, Kanehira M, Ebina M, Kikuchi T, Saijo Y, Nukiwa T, and Prockop DJ. Mesenchymal stromal cells protect cancer cells from ROS-induced apoptosis and enhance the Warburg effect by secreting STC1. *Mol Ther* 20: 417–423, 2012.
26. Ohkouchi S, Ono M, Kobayashi M, Hirano T, Tojo Y, Hisata S, Ichinose M, Irokawa T, Ogawa H, and Kurosawa H. Myriad functions of stanniocalcin-1 (STC1) cover multiple therapeutic targets in the complicated pathogenesis of idiopathic pulmonary fibrosis (IPF). *Clin Med Insights Circ Respir Pulm Med* 9: 91–96, 2015.
27. Ono M, Ohkouchi S, Kanehira M, Tode N, Kobayashi M, Ebina M, Nukiwa T, Irokawa T, Ogawa H, Akaike T, Okada Y, Kurosawa H, Kikuchi T, and Ichinose M. Mesenchymal stem cells correct inappropriate epithelial-mesenchyme relation in pulmonary fibrosis using stanniocalcin-1. *Mol Ther* 23: 549–560, 2015.
28. Pan LF, Yu L, Wang LM, He JT, Sun JL, Wang XB, Bai ZH, Su LJ, and Pei HH. The toll-like receptor 4 antagonist transforming growth factor-beta-activated kinase(TAK)-242 attenuates taurocholate-induced oxidative stress through regulating mitochondrial function in mice pancreatic acinar cells. *J Surg Res* 206: 298–306, 2016.
29. Pearce EJ and Everts B. Dendritic cell metabolism. *Nat Rev Immunol* 15: 18–29, 2015.
30. Sheikh-Hamad D. Mammalian stanniocalcin-1 activates mitochondrial antioxidant pathways: new paradigms for regulation of macrophages and endothelium. *Am J Physiol Renal Physiol* 298: F248–F254, 2010.
31. Siner JM, Jiang G, Cohen ZI, Shan P, Zhang X, Lee CG, Elias JA, and Lee PJ. VEGF-induced heme oxygenase-1 confers cytoprotection from lethal hyperoxia in vivo. *FASEB J* 21: 1422–1432, 2007.
32. Suliman HB, Sweeney TE, Withers CM, and Piantadosi CA. Co-regulation of nuclear respiratory factor-1 by NFkappaB and CREB links LPS-induced inflammation to mitochondrial biogenesis. *J Cell Sci* 123: 2565–2575, 2010.
33. Takyar S, Zhang Y, Haslip M, Jin L, Shan P, Zhang X, and Lee PJ. An endothelial TLR4-VEGFR2 pathway mediates lung protection against oxidant-induced injury. *FASEB J* 30: 1317–1327, 2016.
34. Uebelhoer M and Iruela-Arispe ML. Cross-talk between signaling and metabolism in the vasculature. *Vascul Pharmacol* 83: 4–9, 2016.
35. Wagner GF, Hampong M, Park CM, and Copp DH. Purification, characterization, and bioassay of teleocalcin, a glycoprotein from salmon corpuscles of Stannius. *Gen Comp Endocrinol* 63: 481–491, 1986.
36. Wang Y, Huang L, Abdelrahim M, Cai Q, Truong A, Bick R, Poindexter B, and Sheikh-Hamad D. Stanniocalcin-1 suppresses superoxide generation in macrophages through induction of mitochondrial UCP2. *J Leukoc Biol* 86: 981–988, 2009.
37. Westberg JA, Serlachius M, Lankila P, and Andersson LC. Hypoxic preconditioning induces elevated expression of stanniocalcin-1 in the heart. *Am J Physiol Heart Circ Physiol* 293: H1766–H1771, 2007.
38. Yeung BH and Wong CK. Stanniocalcin-1 regulates re-epithelialization in human keratinocytes. *PLoS One* 6: e27094, 2011.
39. Zhang X, Shan P, Jiang D, Noble PW, Abraham NG, Kappas A, and Lee PJ. Small interfering RNA targeting heme oxygenase-1 enhances ischemia-reperfusion-induced lung apoptosis. *J Biol Chem* 279: 10677–10684, 2004.
40. Zhang X, Shan P, Jiang G, Cohn L, and Lee PJ. Toll-like receptor 4 deficiency causes pulmonary emphysema. *J Clin Invest* 116: 3050–3059, 2006.
41. Zhang X, Shan P, Qureshi S, Homer R, Medzhitov R, Noble PW, and Lee PJ. Cutting edge: TLR4 deficiency

confers susceptibility to lethal oxidant lung injury. *J Immunol* 175: 4834–4838, 2005.
42. Zhang Y, Jiang G, Sauler M, and Lee PJ. Lung endothelial HO-1 targeting in vivo using lentiviral miRNA regulates apoptosis and autophagy during oxidant injury. *FASEB J* 27: 4041–4058, 2013.
43. Zhang Y, Sauler M, Shinn AS, Gong H, Haslip M, Shan P, Mannam P, and Lee PJ. Endothelial PINK1 mediates the protective effects of NLRP3 deficiency during lethal oxidant injury. *J Immunol* 192: 5296–5304, 2014.
44. Zhang Y, Shan P, Srivastava A, Jiang G, Zhang X, and Lee PJ. An endothelial Hsp70-TLR4 axis limits Nox3 expression and protects against oxidant injury in lungs. *Antioxid Redox Signal* 24: 991–1012, 2016.
45. Zhang Y, Zhang X, Shan P, Hunt CR, Pandita TK, and Lee PJ. A protective Hsp70-TLR4 pathway in lethal oxidant lung injury. *J Immunol* 191: 1393–1403, 2013.
46. Zlot C, Ingle G, Hongo J, Yang S, Sheng Z, Schwall R, Paoni N, Wang F, Peale FV, Jr., and Gerritsen ME. Stanniocalcin 1 is an autocrine modulator of endothelial angiogenic responses to hepatocyte growth factor. *J Biol Chem* 278: 47654–47659, 2003.

Address correspondence to:
Dr. Patty J. Lee
Section of Pulmonary, Critical Care and Sleep Medicine
Yale University School of Medicine
PO Box 208057
New Haven, CT 06520-8057

E-mail: patty.lee@yale.edu

Date of first submission to ARS Central, January 22, 2018; date of final revised submission, June 20, 2018; date of acceptance, June 24, 2018.

Abbreviations Used

αSMA = alpha smooth muscle actin
2-NBDG = 2-(*N*-(7-Nitrobenz-2-oxa-1,3-diazol-4-yl)Amino)-2-deoxyglucose
Ad-Ctrl = adenovirus-control (CMV-null)
Ad-Hsp70 = adenoviral Hsp70
ALI = acute lung injury
ARDS = acute respiratory distress syndrome
ATP = adenosine triphosphate
BAL = bronchoalveolar lavage
CC10 = rat 10-kDa Clara cell promoter
CD31 = cluster of differentiation 31
DAPI = 4′,6-diamidino-2-phenylindole
DHE = dihydroethidium
ECAR = extracellular acidification rate
EMSA = electromobility shift assay
ER = endoplasmic reticulum
FACS = fluorescence-activated cell sorter
FCCP = carbonyl cyanide-4-(trifluoromethoxy) phenylhydrazone
HALI = hyperoxia-induced acute lung injury
HSD = honestly significant difference
Hsp70 = heat-shock protein 70
LDH = lactate dehydrogenase
MLEC = mouse lung endothelial cell
NFκB = nuclear factor kappa-light-chain-enhancer of activated B cells
OCR = oxygen consumption rate
PBS = phosphate-buffered saline
PER = proton efflux rate
RA = room air
ROS = reactive oxygen species
RT-PCR = reverse transcription–polymerase chain reaction
SD = standard deviation
sh = silencing RNA
shRNA = small hairpin RNA
siRNA = small interfering RNA
SP-C = surfactant protein C
STC1 = stanniocalcin 1
TEM = transmission electron microscopy
TLR4 = toll-like receptor 4
Trif = TIR-domain-containing adapter-inducing interferon-β
UCP2 = uncoupling protein 2
WT = wild type